

Assessing the ammonium nitrate formation regime in the Paris megacity and its representation in the CHIMERE model

H. Petetin^{1,*}, J. Sciare^{2,3}, M. Bressi², A. Rosso⁴, O. Sanchez⁴, R. Sarda-Estève², J.-E. Petit^{2,**}, and M. Beekmann¹

(1) {LISA/IPSL, Laboratoire Inter-universitaire des Systèmes Atmosphériques, UMR CNRS 7583, Université Paris Est Créteil (UPEC) and Université Paris Diderot (UPD), France}

(2) {LSCE, Laboratoire des Sciences du Climat et de l'Environnement, CNRS-CEA-UVSQ, Gif-sur-Yvette, France}

(3) {Energy Environment Water Research Center (EEWRC), The Cyprus Institute, Nicosia, Cyprus}

(4) {AIRPARIF, Agence de surveillance de la qualité de l'air, Paris, France}

* now at: Laboratoire d'Aérologie, Université Paul Sabatier and CNRS, Toulouse, France

** now at: Air Lorraine, Villers-les-Nancy, France

Correspondence to: H. Petetin (hervepetetin@gmail.com)

Abstract

Secondary inorganic compounds represent a major fraction of fine aerosol in the Paris megacity. The thermodynamics behind their formation is now relatively well constrained, but due to sparse direct measurements of their precursors (in particular NH_3 and HNO_3), uncertainties remain on their concentrations and variability as well as the formation regime of ammonium nitrate (in terms of limited species, among NH_3 and HNO_3) in urban environments such as Paris. This study presents the first urban background measurements of both inorganic aerosol compounds and their gaseous precursors during several months within the city of Paris. Intense agriculture-related NH_3 episodes are observed in spring/summer while HNO_3 concentrations remain relatively low, even during summer, which leads to a NH_3 -rich regime in Paris. The local formation of ammonium nitrate within the city appears low, despite high NO_x emissions. The dataset also allows evaluating the CHIMERE chemistry-transport model (CTM). Interestingly, the rather good results obtained on ammonium nitrates hide significant errors on gaseous precursors (e.g. mean bias of -75 and +195% for NH_3 and HNO_3 , respectively). This leads to a mis-representation of the nitrate formation regime

through a highly underestimated Gas Ratio metric (introduced by Ansari and Pandis (1998)) and a much higher sensitivity of nitrate concentrations to ammonia changes. Several uncertainty sources are investigated, pointing out the importance of better assessing both NH_3 agricultural emissions and OH concentrations in the future. These results finally remind the caution required in the use of CTMs for emission scenario analysis, highlighting the importance of prior diagnostic and dynamic evaluations.

1 Introduction

Atmospheric particulate matter (PM) consists in a complex mixture of various organic and inorganic compounds known for causing serious adverse effects on human health (Chow, 2006; Pope et al., 2009), in particular close to primary sources in urban environments. Through acidic deposition, it also affects both ecosystems (Camargo and Alonso, 2006; Grantz et al., 2003) and monuments (Lombardo et al., 2013). It plays a crucial but still uncertain role in climate change through interactions with radiation and clouds formation, leading at a global scale to a radiative forcing estimated between -1.9 and -0.1 W.m^{-2} at a 95% confidence interval (IPCC, 2013). Among the various chemical constituents of PM, nitrate (NO_3^-) contributes significantly in the form of semi-volatile ammonium nitrate to the fine (PM with aerodynamic diameter below $2.5 \mu\text{m}$) and coarse (between 2.5 and $10 \mu\text{m}$) aerosol modes, with mean contributions in Europe around 6-16 and 6-20%, respectively (Putaud et al., 2010). Several studies have reported increasing ammonium nitrate relative contributions with increasing PM mass concentrations at urban sites, thus underlying their importance in exceedances of ~~PM~~ European standards (Putaud et al., 2010; Yin and Harrison, 2008). Such a pattern has been evidenced for the city of Paris by Sciare et al. (2010), Bressi et al. (2013) and Petit et al. (2015) and clearly points to the need for a better understanding of the processes controlling the formation of ammonium nitrate.

Ammonium nitrate formation primarily results from both the formation of nitric acid (HNO_3) and the emission of ammonia (NH_3) under favorable thermodynamic conditions. NO_2 is converted into HNO_3 through ~~the~~ oxidation by the OH radical (homogeneous direct pathway) or ozone (through the formation of several intermediate compounds, including nitrate radical NO_3 and nitrogen pentoxide N_2O_5 ; heterogeneous indirect pathway) (Seinfeld and Pandis, 2006). The first pathway is expected to dominate during daytime, when OH concentrations are the highest (Matsumoto and Tanaka, 1996). Conversely, due to the very short lifetime of the NO_3^* radical in the presence of solar irradiation (Vrekoussis et al., 2004), the second pathway mainly acts during nighttime, favored by decreasing temperature and increasing relative humidity (RH), or during fog events ((Platt et al., 1981); Dall'Osto et al., 2009; Healy et al., 2012). Additionally, some HNO_3 may also be directly emitted by both anthropogenic (~~e.g. industry~~) and natural (e.g. volcanoes, Mather et al., 2004) sources. NH_3 is mainly emitted by agricultural activities (at 93% in France, CITEPA (2013)), with

several other minor sources including industry, traffic (e.g. Kean et al., 2009; Bishop et al., 2010; Carslaw and Rhys-Tyler, 2013; Yao et al., 2013) or sewage disposal (Sutton et al., 2000). In the presence of NH_3 available after the neutralization of sulfate, a thermodynamic equilibrium is engaged between ~~both gaseous compounds~~ (HNO_3 and NH_3). It potentially leads to the formation of NH_4NO_3 in the aqueous or solid phase, depending on temperature, RH and sulfate concentrations (Ansari and Pandis, 1998; Mozurkewich, 1993). In marine environments, HNO_3 may also adsorb onto NaCl salts and react to form sodium nitrate (NaNO_3) in the coarse fraction (Harrison and Pio, 1983; Ottley and Harrison, 1992). The relationship between nitrate aerosols and its gaseous precursors is thus highly non-linear (Ansari and Pandis, 1998), and the calculation of nitrate concentrations requires the use of thermodynamic models able to determine the partitioning of inorganic compounds between the gaseous and aerosol (aqueous or solid) phases depending on the temperature and RH conditions (see Fountoukis and Nenes, 2007 for a review).

Considering the high contribution of nitrate to fine particulate pollution, both the identification of the limited species (among NH_3 and HNO_3) in the formation of NH_4NO_3 and the quantification of the PM response to a given emission reduction of either precursor are crucial information for air quality management authorities in charge of designing efficient PM control strategies. Various approaches have been proposed in the literature to investigate these points, the reliability of results mostly depending on the observational dataset available. As they do not require any measurements, chemistry-transport models (CTMs) simulations and emission reduction scenarios remain the easiest way to provide a first guess of the limited species and PM response to emission changes.

Over Europe, several studies with different CTMs have simulated a HNO_3 -limited regime (Sartelet et al., 2007 and Kim et al., 2011 with the POLYPHEMUS model; Hamaoui-Laguel et al., 2014 with the CHIMERE model; Pay et al., 2012 with the CALIOPE-EU modelling system). However, such an approach relies on the good performance of CTMs that still suffer from various uncertainties, in particular in their input data (e.g. emission inventories). In respect to these perspectives, comparisons with field observations are highly valuable for evaluating model outputs. When measurements of total nitrate ($\text{TNO}_3 = \text{HNO}_{3(\text{g})} + \text{NO}_3^-$), total ammonia ($\text{TNH}_3 = \text{NH}_{3(\text{g})} + \text{NH}_4^+$) and total sulfate ($\text{TS} = \text{H}_2\text{SO}_{4(\text{g})} + \text{HSO}_4^- + \text{SO}_4^{2-}$) are available, it is possible to diagnose which precursor is limiting nitrate formation. A first approach relies on the use of the gas ratio (GR) defined as the ratio of free ammonia after sulfate neutralization ($\text{FNH}_x (\mu\text{mol m}^{-3}) = \text{NH}_3 + \text{NH}_4^+ - 2 \times \text{SO}_4^{2-}$) over total nitrate ($\text{TNO}_3 (\mu\text{mol m}^{-3}) = \text{HNO}_3 + \text{NO}_3^-$) (Ansari and Pandis, 1998). GR values above unity indicate a regime mainly limited by HNO_3 (e.g. NH_3 -rich regime) in which there is enough NH_3 to neutralize both sulfate and nitrate. Conversely, GR between zero and one indicate that there is enough NH_3 to neutralize sulfate but not nitrate, while negative ones correspond to a NH_3 -poor regime in which NH_3 amounts are insufficient to even neutralize sulfate. Based on the ~~EMEP~~ (European Monitoring and Evaluation Program) regional background observations, Pay et al. (2012) have obtained GR

1 above unity (i.e. a HNO_3 -limited regime) over continental Europe, in reasonable agreement with the
2 CALIOPE model. Conversely, a NH_3 -limited regime was found over ocean and closer to coasts in
3 some countries (e.g. Spain, England, countries around Baltic Sea) due to ship emissions of SO_2 and
4 NO_x and low NH_3 over marine regions. However, the determination of the limited compound based
5 on GR is valid only under the assumption of a complete transfer (of the limited species) in the
6 aerosol phase (i.e. at low temperature and high RH). Under ambient conditions favoring a
7 partitioning between both phases, both NH_3 and HNO_3 exist in the gas phase and the nitrate
8 formation may be sensitive to changes in one or the other precursor. A more realistic assessment of
9 the nitrate formation regime can be obtained by performing sensitivity tests on thermodynamic
10 models fed by field measurements (concentrations, temperature and RH). Such an approach allows
11 quantifying the PM response to total reservoir (either TNH_3 , TNO_3 or TS) concentrations reductions
12 (Ansari and Pandis, 1998 and Takahama et al., 2004 with the GFEMN model; Blanchard and Hidy,
13 2003 with the SCAPE2 model). These studies rely on the hypothesis that the concentration
14 reduction of one specific compound does not affect the others, which is not true due to lifetime
15 differences between gas and aerosol phases induced by contrasted deposition rates; for instance, a
16 reduction of sulfate increases the amount of FNH_x available for the formation of nitrate that deposit
17 less than HNO_3 (Davidson and Wu, 1990), which finally increases the TNO_3 reservoir. These
18 difficulties may be overcome through the combined use of observations and deposition
19 parameterizations in observation-based box models (Vayenas et al., 2005). As such models cannot
20 integrate the whole complexity at stake in the atmosphere, CTMs are still needed to assess the
21 nitrate formation regime and the PM response to precursors changes, but require in turn to be
22 validated by experimental data.

23 This paper aims at investigating the variability and sources of both HNO_3 and NH_3 , and the
24 associated NH_4NO_3 formation regime in the Paris megacity, as well as the ability of the CHIMERE
25 regional CTM to reproduce it. To this end, an important experimental effort, in the framework of
26 the PARTICULES and FRANCIPOL projects, has recently made available a large database of fine
27 aerosol chemical compounds (e.g. nitrate, ammonium, sulfate) and inorganic gaseous precursors
28 (e.g. HNO_3 , NH_3) in the region of Paris. To our knowledge, this is the first time that simultaneous
29 measurements of inorganic compounds in both gaseous and aerosol phases, covering most seasons
30 are performed in France. Experimental aspects are described in Sect. 2. The CHIMERE model and
31 its setup is then introduced in Sect. 3. Results are shown and discussed in Sect. 4, while overall
32 conclusions are given in Sect. 5.

2 Experimental

2.1 Fine aerosols measurements

As part of the AIRPARIF-LSCE “PARTICULES” project (Airparif, 2011, 2012), fine aerosol particles ($\text{PM}_{2.5}$) were collected every day during 24 h (from 00:00 to 23:59 LT) during one year (from 11 September 2009 to 10 September 2010) using two collocated Leckel low volume samplers (SEQ47/50) running at $2.3 \text{ m}^3 \text{ h}^{-1}$. One Leckel sampler was equipped with quartz filters (QMA, Whatman, 47 mm diameter) for carbon analyses, the second with Teflon filters (PTFE, Pall, 47 mm diameter, $2.0 \text{ }\mu\text{m}$ porosity) for gravimetric and ion measurements (including NH_4^+ , NO_3^- , SO_4^{2-}). Six sampling sites were implemented, covering the region of Paris. Only the results for the background station located in the city center of Paris (4th district, $48^\circ 50' 56'' \text{N}$, $02^\circ 21' 55'' \text{E}$, 20 m above ground level, a.g.l.) will be presented here. More information on the experimental setup and quality control of the datasets is available in Bressi et al. (2013). Note that filter measurements are subject to artefacts, through the evaporation and/or the adsorption of semi-volatile compounds (Pang et al., 2002), and thus mostly affect ammonium nitrate and organic matter concentrations. Daily chemical mass closure studies and comparisons with on-line artefact-free measurements were performed for that purpose and showed that filter sampling was ~~missing quite~~ systematically about 20% of $\text{PM}_{2.5}$ (15% of fine nitrate; Bressi et al., 2013).

2.2 Gaseous precursors measurements

As part of the PRIMEQUAL (*Programme de Recherche Interorganisme pour une MEilleure QQualité de l'Air à l'échelle Locale*) « FRANCIPOL » project, gaseous precursors (NH_3 , HNO_3 , SO_2) were monitored in near real-time on the roof platform (14 m a.g.l.) at the Laboratoire d'Hygiène de la Ville de Paris (LHVP) in the heart of Paris (13th district). Gas-phase NH_3 measurements were obtained for a 10-month period (May 2010 – February 2011) every 5 min using an AiRRmonia monitor (Mechatronics Instruments BV, The Netherlands). The March/April periods (2010 and 2011) were missing due to technical problems of the instrument. Based on conductivity detection of NH_4^+ , gaseous NH_3 were sampled at 1 L min^{-1} using a 1-m long Teflon (1/2 inch diameter) sampling line. ~~Then, it was~~ collected through a sampling block equipped with an NH_3 -permeable membrane; a demineralized water counter-flow allows NH_3 to solubilize in NH_4^+ . A second purification step was applied by adding 0.5 mM sodium hydroxide, leading to the detection of NH_4^+ in the detector block. The instrument ~~has~~ been calibrated regularly (twice per months) using 0 ppb and 500 ppb NH_4^+ aqueous solution (NIST standards). Two sets of sampling syringes ensure a constant flow throughout the instrument, but also create a temporal shift, ranging from 10 to 40 min for different studies (Erisman et al., 2001; Cowen et al., 2004; Zechmeister-Boltenstern, 2010; von Brobrutzki et al., 2010). We have taken here a constant value of 30 min for this delay in

time response. Detection limit and precision of the instrument are typically $0.1 \mu\text{g m}^{-3}$ and 3 to 10%, respectively (Erisman et al., 2001; Norman et al., 2009). More than 62,000 valid data points of NH_3 - covering 217 days - were obtained with the AiRRmonia instrument and used for this study. HNO_3 and SO_2 were analyzed continuously for an 11-month period (March 2010 – January 2011) using a Wet Annular Denuder (WAD) similar to the one reported in details by Trebs et al. (2004) and coupled with Ion Chromatography (IC). Briefly, whole air was sampled at $\sim 10 \text{ L min}^{-1}$ in the WAD. This air flowrate – slightly below the 17 L min^{-1} usually set – was taken to ensure a laminar flow and minimize particle losses onto the walls of the WAD and thus minimize possible artefacts in our IC (anion) measurements that could raise from inorganic salts present in the particulate phase. Following the recommendations by Neuman et al. (1999), our sampling line were made of plastic (PE, 1/2 inch diameter, John Guest, USA) and reduced to 1 m in order to keep a residence time of sampled air below 1s preventing formation/losses of NH_4NO_3 (Dlugi 1993). $18.2 \text{ M}\Omega$ water was used to rinse the WAD at a flowrate of $\sim 0.40 \text{ ml min}^{-1}$ and feed the IC with the solubilized acid gases. The IC (ICS2000, Dionex) configuration setup is similar to the one reported by (Sciare et al., 2011). Time resolution (chromatogram) was typically 15 min for the major gaseous acidic species (HCOOH , CH_3COOH , HCl , HONO , HNO_3 , SO_2). Oxidation of SO_2 into SO_4^{2-} in the liquid flow downstream of the WAD was performed by solubilization of ambient oxidants such as H_2O_2 . Based on these settings, detection limit for acidic gases was typically below $0.1 \mu\text{g m}^{-3}$. Uncertainties in ambient concentrations of acidic gases depend on air and liquid flowrates (controlled on a weekly basis) as well as the IC calibration (performed every 2 months). Overall standard deviations (1σ) of 6%, 15% and 10% were calculated for these 3 parameters (air flowrate, liquid flowrate, IC calibration), respectively, leading a total uncertainty of about 20% for the WAD-IC measurements.

This WAD technique has been successfully intercompared with off-line techniques in (Trebs et al., 2008). Further comparison of the WAD-IC technique was performed during our study with a commercially available SO_2 analyzer (AFM22, Environnement S.A.) for a period of 3 months. Despite the poor detection limit ($1 \text{ ppb} = 2.43 \mu\text{g m}^{-3}$) of the commercially available instrument and the low ambient concentrations recorded at our station with SO_2 monthly means ranging from 0.76 to $3.03 \mu\text{g m}^{-3}$ measured with our WAD-IC instrument, quite consistent results were obtained from this intercomparison (slope of 0.73 and $r^2=0.56$ for $n=1671$ hourly averaged data points). More than 24,000 valid data points of SO_2 and HNO_3 - covering 253 days - were obtained with the WAD-IC instrument and used for this study.

2.3 Meteorological parameters measurement

Beside chemical compounds, traditional meteorological parameters — temperature, wind speed and direction, RH — are also measured at the MONTSOURIS station (2.337°E , 48.822°N) in Paris,

close to the LHVP site (~ 2 km). In addition, boundary layer height (BLH) estimations are retrieved from an aerosol lidar at the SIRTa (*Site Instrumental de Recherche par Télédetection Atmosphérique*) site (48.712°N , 2.208°E) (Haeffelin et al., 2012).

This paper will focus on measurements performed from the 1 April to 31 December 2010. Note that all the measurements described in previous sections come from different campaigns and measurement periods that do not entirely overlap. Measurements of secondary inorganic aerosols (NH_4^+ , NO_3^- , SO_4^{2-}) are available ~~at the daily scale~~ between the 1 April and the 10 September 2010. NH_3 (HNO_3) observations are available ~~at the hourly scale~~ from the 20 May (1 April) to the 31 December 2010.

2.4 Representativeness and datasets combination

The purpose of this study is to investigate the relation of NH_4NO_3 with its gaseous precursors, which ideally requires co-located measurements of all compounds in both phases. This was not the initial purpose of PARTICULES and FRANCIPOL projects, and thus, no such co-located observations are available in Paris. However, we argue here that the two datasets (inorganic aerosols measured in the 4th district of Paris, and gaseous precursors measured in the 13th district) can be reasonably considered as co-located and representative of the urban background of at least the southern half of the Paris city.

Several elements support this hypothesis. **First, both sites are only ~ 3 km away.** Second, both sites are located on the rooftop of rather high buildings (20 and 14 m a.g.l.), thus quite far from direct influence of local pollution sources (e.g. traffic) and at a height where the venting of pollution is favored by the absence of obstacles and likely stronger winds (compared to the street level). The height of the LHVP roof site is slightly lower compared to the other site, but the building is located in a public garden, which further limits the possibility of local contamination by surrounding pollution sources. Third, based on the $\text{PM}_{2.5}$ chemical speciation measurements performed both inside Paris and at several rural sites all around the Paris region during a whole year, the PARTICULES project ~~has allowed to demonstrate~~ that secondary inorganic aerosols in the Paris urban background are mostly imported from outside the city (Petetin et al., 2014). At the annual scale, the contribution of imports was estimated to 78% for nitrate, 90% for ammonium and 98% for sulfates (see Table 6 in Petetin et al., 2014). This is mostly explained by (i) the presence of strong pollution reservoirs in Europe (e.g. Benelux, eastern Europe) from where large plumes can be advected toward Paris ~~in specific~~ meteorological conditions, (ii) the time necessary for the formation of inorganic aerosols (including the oxidation of NO_x and SO_2) is too low to allow a strong local production that thus preferentially occurs downwind in the Paris plume, as observed

during the MEGAPOLI campaign (Freney et al., 2014), and (iii) the limited occurrence of stagnant conditions in Paris (that would let enough time to gaseous precursors to produce inorganic aerosols). The high contribution of imports is confirmed by the comparison of daily inorganic aerosol concentrations between the 4th district site and a traffic site located along the Paris ring 8 km westward, that shows a very good accordance for all inorganic aerosols during the whole year (ammonium: $y=0.95x+0.02$, $R=0.97$, $N=325$; nitrate: $y=0.99x-0.09$, $R=0.98$, $N=325$; sulfate: $y=1.04x+0.01$, $R=0.98$, $N=325$). Thus, concerning secondary inorganic aerosols, the urban background can be considered as rather homogeneous at the scale of the whole Paris agglomeration. And observations in the 4th district of Paris can be reasonably combined to gaseous precursors observations at the other site.

In terms of spatial representativeness for HNO_3 and NH_3 , no other measurements are available to quantitatively assess the homogeneity of their urban background. In particular, some NO_x emitted within the center of the city may be already converted into HNO_3 in the borders of the Paris agglomeration, leading to higher concentrations compared to the center of Paris. Thus, one cannot a priori consider that these measurements are representative of the urban background at the scale of the whole Paris agglomeration. However, as we already discussed, considering the morphology and the geographical location of this LHVP site, one can reasonably consider that it is representative of the urban background of at least the southern half of Paris city.

3 Model setup and input data

3.1 CHIMERE model description

Simulations are performed with the CHIMERE CTM (Schmidt and Derognat, 2001; Bessagnet et al., 2009; Menut et al., 2013) (www.lmd.polytechnique.fr/chimere) designed to provide short-term predictions of ozone and aerosols, as well as to help emissions mitigation assessment through emission reduction scenarios. It is used both in research activities and operational air quality monitoring and forecasting at the local, national and European scale (ESMERALDA over the northern part of France; PREVAIR service, www.prevoir.org; GMES-MACC program).

The CHIMERE model includes the MELCHIOR2 (*ModEle CHImique de l'Ozone à l'échelle Régionale*) chemical mechanism (around 40 species and 120 reactions) for the gas-phase chemistry, some aqueous-phase (e.g. aqueous pathways for sulfate production) and heterogeneous (e.g. HNO_3 formation on existing particles and fog droplets, including the conversion of N_2O_5) reactions, and size dependent aerosol compounds (9 bins ranging from 40 nm to 20 μm diameters), including secondary organic and inorganic aerosols. Dry and wet deposition of gaseous and aerosol species is parameterized from three types of sequential resistances following the resistance analogy (Wesely, 1989). An aerodynamical resistance is estimated based on turbulent parameters (e.g. Monin-

Obukhov length, friction velocity, dynamical roughness length). A quasi-laminary boundary layer resistance is calculated based on the molecular diffusivity of water and gaseous species and Prandtl number. The surface resistance of vegetation and soils is estimated from several parallel resistances related to plant surfaces via opening of stomata, and related to non-stomatal deposition at plant and soil surfaces (Erisman et al., 1994). The scavenging of gases and particles, both in clouds and rain droplets, is included in CHIMERE. The scavenging of HNO_3 and NH_3 by cloud droplets (in rain droplets) is assumed reversible (irreversible). In clouds, particles can be scavenged by coagulation with cloud droplets or by precipitation, or can act as cloud condensation nuclei to form new droplets. Particles can also be scavenged by raining drops below the clouds. More details can be found in (Menut et al., 2013). The model also includes a parameterization of coagulation, absorption and nucleation aerosol processes.

Inorganic species are treated using the ISORROPIA thermodynamic equilibrium model (Nenes et al., 1998), considering only the NH_3 - HNO_3 - H_2SO_4 - H_2O system. ISORROPIA follows a bulk aerosol approach (without any consideration of the aerosol size distribution) and assumes an instantaneous equilibrium in the gas-aerosol system, as well as no influence of other compounds (in particular, the soluble organic matter). Given the temperature, RH, TNO_3 , TNH_3 and TS (assuming that $\text{TS}=\text{SO}_4^{2-}$ due to low concentrations of H_2SO_4 and HSO_3 in the aerosol phase), the partitioning coefficient between both aerosol and gas phases at equilibrium is computed and used to drive the system toward the corresponding direction (thus countering the hypothesis of an instantaneous equilibrium assumed in ISORROPIA). For calculation efficiency, the model is not used on-line but through a tabulated version designed to cover a large range of meteorological conditions with temperature ranging from 260 to 312 K (increment +2.5 K), RH from 0.3 to 0.99 (increment +0.05) and TS, TNO_3 and TNH_3 concentrations from 10^{-2} to $65 \mu\text{g m}^{-3}$ (increment x1.5) (Menut et al., 2013).

3.2 Model configuration

As shown in Fig. 1, three nested domains are considered in all simulations — a large (LAR), a medium (MED) and a fine (FIN) domain —, with horizontal resolutions increasing from $0.5 \times 0.5^\circ$ (roughly $50 \times 50 \text{ km}$), $9 \times 9 \text{ km}$ and $3 \times 3 \text{ km}$, respectively. A discretization of 8 levels, from 40 m to 5 km a.g.l., is applied on the vertical dimension.

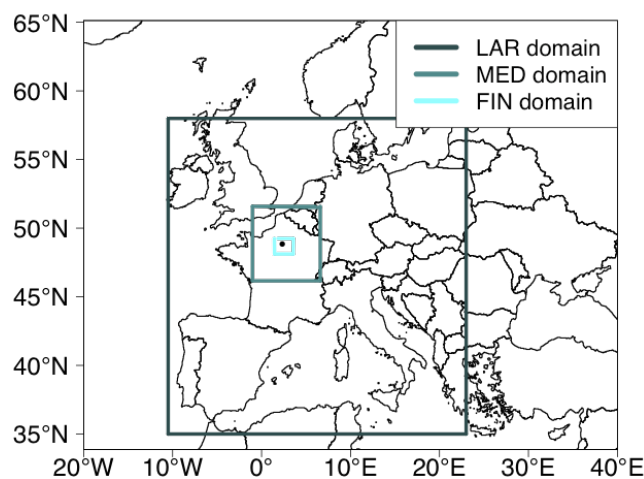


Figure 1: Nested domains (the black points in the finest domain indicates Paris). Resolutions are 0.5x0.5° (LAR domain), 9x9 km (MED) and 3x3 (FIN).

Meteorological inputs are ~~taken from~~ PSU/NCAR MM5 simulations (Dudhia, 1993) using boundary conditions and large scale data coming from Final Analyses (FNL) data from National Centers for Environmental Prediction (NCEP).

Gaseous and aerosol emissions in all domains come from the so-called TNO-MP (MP for MegaPoli) inventory. Developed in the framework of the European MEGAPOLI (Megacity: emission, urban, regional and global atmospheric pollution and climate effect, and integrated tools for assessment and mitigation ; www.megapoli.info) project (Baklanov et al., 2010), this highly-resolved (0.125 x 0.0625°, i.e. roughly 7 x 7 km) European inventory is based on the TNO inventory (Gon et al., 2010; Pouliot et al., 2012; Kuenen et al., 2014), but incorporates bottom-up emission data (compiled by local authorities such as Airparif for Paris (Airparif, 2010)) over the four European megacities (Paris, London, Rhine-Ruhr and Po valley) (see Denier van der Gon et al., 2011; for more details). The region of Paris roughly corresponds to the FIN domain. In order to reach the CHIMERE resolution, emissions are downscaled based on the 1x1 km-resolved GLCF (Global Land Cover Facility) land use database (Hansen et al., 2000), and apportioned according to the type of land use (Menut et al., 2013).

Boundary and initial conditions come from the LMDz-INCA2 (Folberth et al., 2006) global model for gaseous species and the LMDZ-AERO (Folberth et al., 2006; Hauglustaine, 2004) for particulate species. Biogenic emissions are computed from the MEGAN model using parameterizations from Guenther et al. (2006).

This reference simulation will be referred to as the MOD case. A second simulation is performed without any local anthropogenic emissions from the region of Paris (in the three nested domains), in order to assess the influence of imported pollution over the city of Paris. It will be referred to as the MOD-noIDF case (IDF for Ile-de-France ~~which designs~~ the name of the region of Paris). In addition, as NH₃ is strongly impacted by dry deposition which is still poorly constrained in current

CTMs, a third simulation (so-called MOD-nodp) is performed without any NH₃ dry deposition over the entire domain in order to investigate its influence on concentrations within Paris.

4 Results

The following subsections present results on sulfate and SO₂ (Sect. 4.1), NH₃ (Sect. 4.2) and HNO₃ (Sect. 4.3). For all compounds, the temporal variability given by measurements is assessed at different scales (monthly, daily and diurnal), as well as the model ability to reproduce the observed concentrations. For the analysis of air mass origins, back-trajectories have been calculated during the whole period with the FLEXTRA model (Stohl et al., 2001) using the same MM5 meteorology already used in the CHIMERE simulations. Calculations are performed every 6 h with 10 particles distributed around the center of Paris, starting at 500 m altitude, which leads to a daily set of 40 back-trajectories. Several uncertainty sources in the model (or input data) are also discussed. The nitrate formation regime in terms of limiting species among NH₃ and HNO₃, the nitrate simulation in CHIMERE as well as the nitrate response to changes in precursors concentrations are then characterized in Sect. 4.4.

Statistical metrics used in the evaluation of the CHIMERE results compared to observations are defined as follows:

- Mean bias: $MB = \frac{1}{n} \sum_{i=1}^n (m_i - o_i)$ (1)

- Normalized mean bias: $NMB = \frac{\frac{1}{n} \sum_{i=1}^n (m_i - o_i)}{\bar{o}}$ (2)

- Root mean square error: $RMSE = \sqrt{\frac{1}{n} \sum_{i=1}^n (m_i - o_i)^2}$ (3)

- Normalized root mean square error: $RMSE = \frac{\sqrt{\frac{1}{n} \sum_{i=1}^n (m_i - o_i)^2}}{\bar{o}}$ (4)

- Correlation coefficient: $R = \frac{\sum_{i=1}^n (m_i - \bar{m})(o_i - \bar{o})}{\sqrt{\sum_{i=1}^n (m_i - \bar{m})^2 \sum_{i=1}^n (o_i - \bar{o})^2}}$ (5)

With m_i and o_i being the modelled and observed concentrations at time i , respectively, and \bar{m} and \bar{o} their average over a given period.

4.1 Sulfate and SO₂

Sulfate daily concentrations in Paris are given in Fig. 2. The variability of sulfate (as of nitrate) during the PARTICULES campaign has been discussed in details in Bressi et al. (2013). Fine

1 (PM_{2.5}) sulfate concentrations range between 0.4 and 5.0 $\mu\text{g m}^{-3}$ (~~plus~~ one high value at 8.7 $\mu\text{g m}^{-3}$),
2 with an average of 2.0 $\mu\text{g m}^{-3}$ over the studied period (1 April – 10 September). The episodes with
3 highest concentrations are associated ~~to~~ air masses originating from the North/North-East, ~~as~~
4 ~~previously noticed~~ by Bressi et al. (2013), Petetin et al. (2014) and Petit et al. (2015). Despite a
5 faster SO₂-to-sulfate conversion due to higher OH levels in summer, lower concentrations are
6 measured during that season due to a combination of lower SO₂ emissions and a dominant marine
7 regime, with relatively clean air masses originating from West and ~~South-West~~ and slightly more
8 polluted ones from ~~North-West~~.

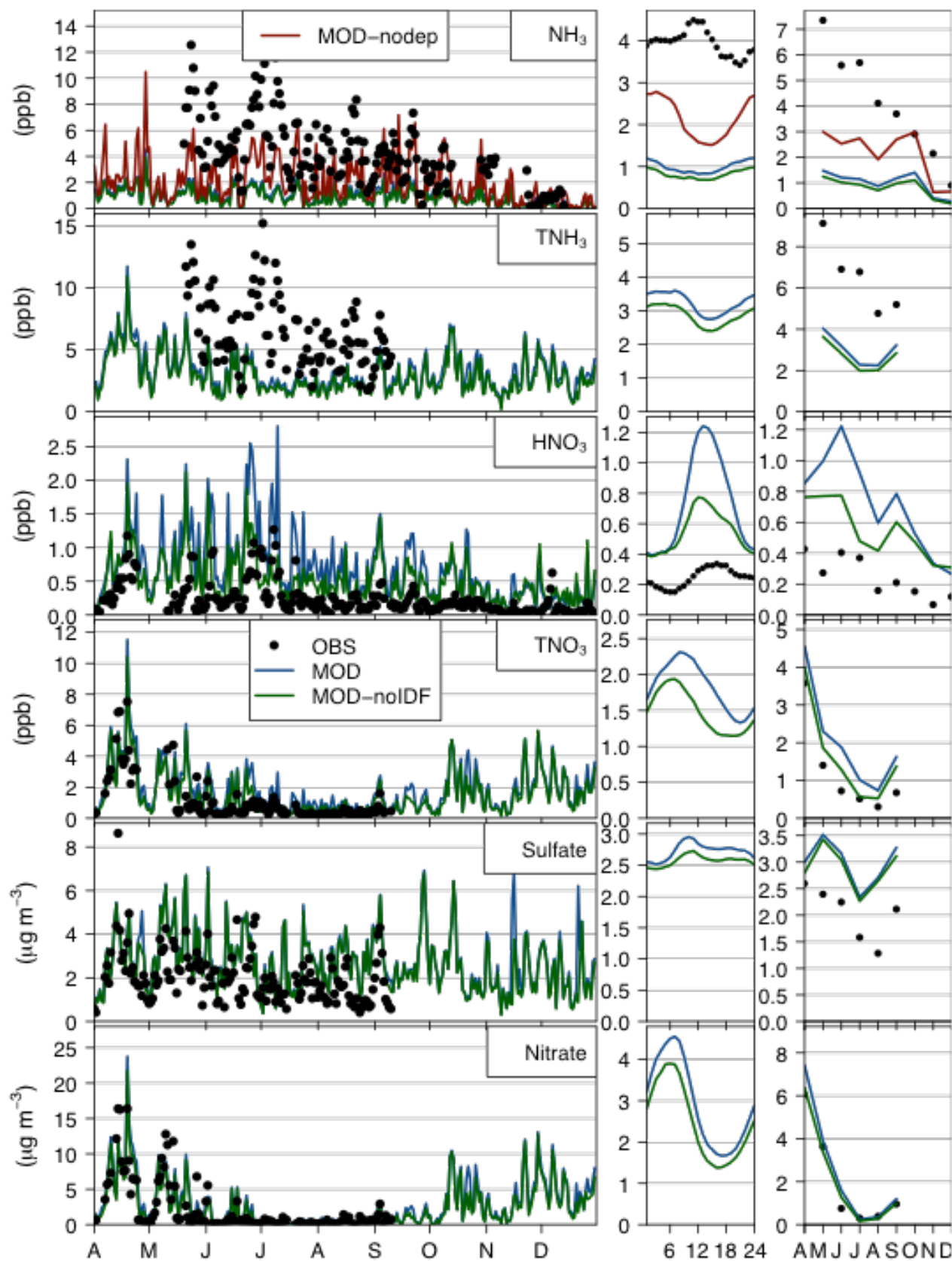


Figure 2: Observed and modelled daily averaged concentrations (left panel), diurnal profiles (middle panel), and monthly concentrations (right panel). MOD-nodep results are only shown for NH_3 . Note: CHIMERE monthly concentrations are computed including only days with available observational data. For particulate matter observations, only daily values are available.

During the period of available data (152 days in spring and summer), NH_3 levels are high enough to fully neutralize both sulfate and nitrate, as indicated by the linear regression of NH_4^+ versus $\text{NO}_3^- + 2\text{SO}_4^{2-}$ daily concentrations in the fine mode that gives a slope of 1.01, a y-intercept of -0.20 ppb and a correlation coefficient (r^2) of 0.97 ($n=150$; see Fig. S1 in the Supplement). Note that plotting all major cations ($\text{Na}^+ + \text{NH}_4^+ + \text{K}^+ + 2\text{Ca}^{2+} + 2\text{Mg}^{2+}$) against all major anions ($\text{NO}_3^- + 2\text{SO}_4^{2-} + \text{Cl}^-$) leads to a slope of 1.03, a y-intercept of +0.13 ppb and a correlation of 0.97, demonstrating the neutrality of our fine aerosol.

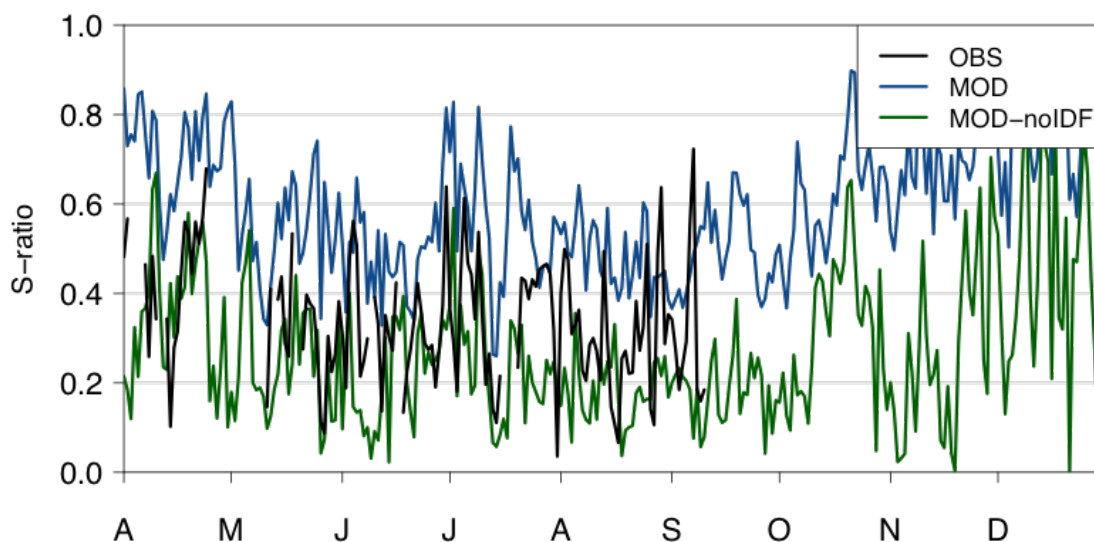


Figure 3: Observed and modelled (with – MOD case – and without – MOD-noIDF case – emissions over the Paris region) daily S-ratio in Paris.

Statistical results of modelled versus measured concentrations are reported in Table 1. The model partially reproduces the day-to-day variability of sulfate concentrations ($r=0.59$), but gives overestimated concentrations, with a NMB of +48% and a NRMSE of 74%. This does not appear to be related to a too high SO_2 -to-sulfate conversion since SO_2 concentrations are significantly overestimated in Paris, by about a factor of 3 (Table 1). This is also suggested by the simulated S-ratio. This indicator – defined as the ratio of SO_2 over $\text{SO}_2 + \text{SO}_4^{2-}$, all concentrations being expressed in $\mu\text{g m}^{-3}$ (Hass et al., 2003; Pay et al., 2012) – allows to assess how fresh is a plume containing sulfur. High S-ratios are found in air masses containing freshly emitted SO_2 , while low S-ratios are associated to older air masses in which more SO_2 have already been converted into sulfates. The observed and simulated S-ratios are shown in Fig. 3 (the $\text{SO}_2 + \text{SO}_4^{2-}$ time series is shown in Fig. S4 in the Supplement). In the MOD simulation, CHIMERE clearly overestimates the S-ratio (average value of 0.54 against 0.34 in the observations, i.e. a positive bias of +60%), i.e. the simulated air masses contain too much freshly emitted SO_2 compared to reality. Such a high bias on SO_2 concentrations is not expected, but does not appear representative of the CHIMERE performance at a larger scale. Considering the SO_2 observations available at 9 urban background sites (AIRPARIF operational network) in the region of Paris, NMB are lower, ranging from +24 to +160%. As a large part of SO_2 is emitted by point sources, the dilution effect in a 3×3 km cell

remains a well-known uncertainty source at stations potentially impacted by plumes coming from nearby industrial facilities. However, in our case, large SO₂ industrial point sources are relatively far from our background urban station, and emissions from non-point sources (i.e. emissions in road transport and residential sectors) remain important in the center of Paris, which suggests potential errors on the Paris agglomeration emissions (overestimation of total emissions, wrong vertical allocation) and/or the BLH. Indeed, the average SO₂ diurnal profile shows maximum discrepancies (up to a factor of 4.8) during the transition from a convective to a nocturnal boundary layer. As this transition occurs too early in the model (see Fig. S3 in the Supplement), this likely explains a noticeable part of the bias on SO₂. Conversely, the sulfate overestimation may be due to errors during the transport of air masses from North-Eastern Europe.

Table 1: Statistical results at our urban background sites over the whole period (all statistical metrics are defined at the beginning of Sect. 4; MO is the observed concentration mean, N the data coverage).

Species	Case	MO	MB	NMB	NRMSE			
				(%)	RMSE	(%)	R	N (%)
NH ₃ * (ppb)	MOD	4.0	-3.0	-75	3.9	99	0.42	64
	MOD-noIDF		-3.1	-79	4.1	103	0.39	64
	MOD-noddep		-1.8	-46	3.2	82	0.45	64
HNO ₃ * (ppb)	MOD	0.3	+0.5	+195	0.8	320	0.56	81
	MOD-noIDF		+0.3	+120	0.6	219	0.36	81
SO ₂ * (ppb)	MOD	0.5	+1.0	+194	1.6	303	0.38	83
	MOD-noIDF		-0.1	-20	0.9	170	0.25	83
Ammonium (µg m ⁻³)	MOD	1.2	+0.4	+35	0.9	70	0.84	54
	MOD-noIDF		+0.3	+23	0.8	64	0.84	54
Nitrate (µg m ⁻³)	MOD	2.1	+0.4	+19	2.2	109	0.81	54
	MOD-noIDF		+0.0	+1	2.1	101	0.81	54
Sulfate (µg m ⁻³)	MOD	2.0	+1.0	+48	1.5	74	0.59	54
	MOD-noIDF		+0.9	+42	1.4	69	0.61	54
F-NH _x (ppb)	MOD	5.5	-4.1	-75	4.7	87	0.51	37
	MOD-noIDF		-4.4	-80	5.0	92	0.48	37
S-ratio	MOD	0.3	+0.2	+60	0.3	73	0.46	48
	MOD-noIDF		-0.1	-29	0.2	55	0.33	48
GR (ppb ppb ⁻¹)	MOD	12.6	-11.4	-90	14.2	112	0.37	36
	MOD-noIDF		-11.2	-88	14.0	111	0.33	36

TNH ₃ (ppb)	MOD	6.4	-3.6	-56	4.4	70	0.43	37
	MOD-noIDF		-3.9	-61	4.7	74	0.40	37
TNO ₃ (ppb)	MOD	1.1	+0.8	+71	1.3	123	0.78	47
	MOD-noIDF		+0.3	+31	1.1	97	0.79	47

* Statistics based on hourly data (otherwise, daily data are used).

4.2 Ammonia

4.2.1 Temporal variability

Daily averaged concentrations and diurnal profiles of NH₃ are given in Fig. 2. The model results will be discussed in the next section. According to the review of Reche et al. (2012), NH₃ concentrations in worldwide urban environments range between 0.4 and 63.6 ppb, thus spanning over two orders of magnitude. On a logarithmic scale, the average concentration of 4.0 ppb measured in Paris over the whole period is roughly in the middle range of this range. It is also consistent with the values obtained in other European cities: 4.4 ppb in Aveiro (Portugal, August-May), 5.2 ppb in Roma (Italy, May-March), 5.5 ppb in Münster (Germany, May-June), 3.2 in Thessaloniki (Greece, year), 3.9-10.6 in Barcelona (Spain, July and January), 3.1 ppb in Schiedam (The Netherlands, winter) (Reche et al., 2012 and references therein). NH₃ concentrations in Paris show a large variability (illustrated by a standard deviation of 2.8 ppb) with several intense episodes in late spring and early summer (hourly concentrations reaching up to 18.5 ppb in June), moderate concentrations in late summer and lower ones in autumn and winter. On average, the observed NH₃ diurnal profile (Fig. 2) is rather flat, with slightly increasing concentrations in the morning leading to a maximum at 10:00-13:00 UTC. Concentrations decrease in the afternoon up to a minimum at 20:00 UTC. The diurnal variability of NH₃ depends on many factors, including the strength of local emission sources, the dry deposition, the evolution of the BLH, the formation of NH₄NO₃ during the night promoted by larger RH and its thermodynamically driven evaporation during the daytime (Wichink Kruit et al., 2007). The daytime increase may be partly due to this volatilization of NH₄NO₃.

4.2.1.1 Influence of temperature

Figure 4 shows the NH₃ concentrations in function of the temperature. Both appear clearly linked in Paris, the highest episodes occurring concomitantly with the warmest conditions (see the meteorology evaluation in the Supplement, Sect. S.2). The lower sensitivity to temperature in the model will be discussed later. Such a relation between NH₃ and the temperature has already been observed in other cities (e.g. Perrino et al., 2002; Gong et al., 2011; Reche et al., 2012). Temperature and RH strongly influence the equilibrium constant governing the partitioning of inorganic compounds between the gas and aerosol phases, with higher NH₃ concentrations expected

when the temperature is high and the RH is low, due to the volatilization of NH_4NO_3 . In addition, several NH_3 emission sources may be enhanced by high temperature, including the agricultural (e.g. volatilization of fertilizer) or biological sources.

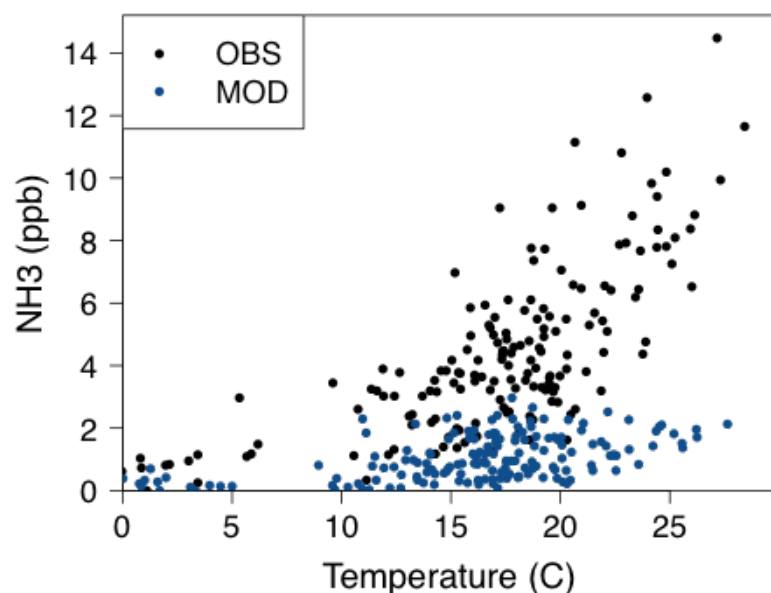


Figure 4: Daily observed (respectively modelled) NH_3 concentrations against observed (respectively modelled) temperature in Paris (for the model, only days with available observations are plotted).

The link between NH_3 and temperature can be illustrated by the early July episode when, in parallel with the temperature increase between 30 June and 2 July, the NH_3 baseline progressively increases in Paris, up to 18.5 ppb at the hourly scale (the maximum over the whole FRANCIPOL period). A part of the NH_3 increase is likely due to evaporation of NH_4NO_3 but in early July, a similar episode is observed on TNH_3 , which means that an additional NH_3 source is at stake. The NH_3/TNH_3 ratios are shown in Fig. 5. The experimentally determined TNH_3 is clearly dominated by NH_3 that has a contribution around 55-99% (83% on average) (again, model results are discussed in Sect. 4.2.2). Negative artefacts on NH_4^+ filter measurements cannot be excluded (in particular during summertime), but increasing NH_4^+ concentrations by 50% has a very limited impact (NH_3 contributions ranging in that case around 45-99%, and 78% on average).

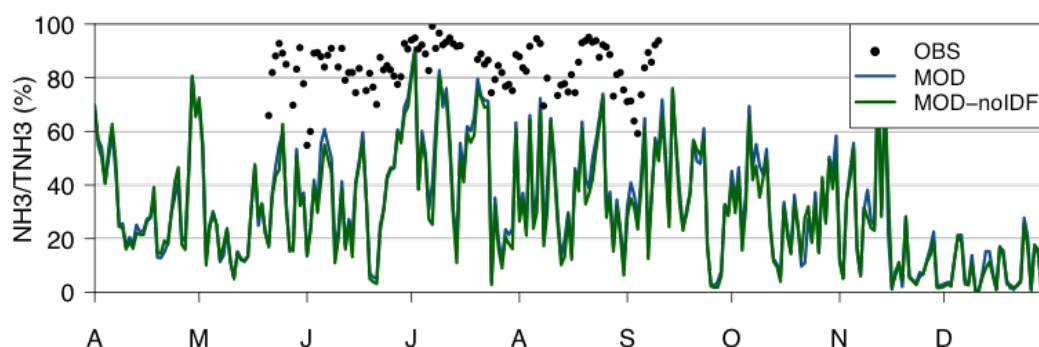


Figure 5: Daily NH_3/TNH_3 ratios in observations (points) and simulations (colored lines).

4.2.1.2 Influence of traffic NH₃

Several studies have previously addressed the question of the NH₃ emitted by the traffic in urban areas, although with more or less contrasted and definitive conclusions depending on the city (e.g. Perrino et al., 2002; Gong et al., 2011). The difficulty notably arises from the short lifetime of NH₃ that can quickly deposit on the ground, be diluted or converted into NH₄⁺. In Paris, the diurnal profile does not show any peak at morning and evening rush hours, even during periods of lower agricultural emissions (e.g. August and September; too few data in winter). This suggests that traffic emissions are probably a relatively minor source during our study. This is supported by the low correlation of BC (mainly emitted by the traffic) and NH₃ concentrations measured at the LHVP site ($r=0.20$ over the whole period). However, it is worth noting that during the end of June episode, the hourly time series shows some morning peaks (above an increasing background line likely due to the advection of agricultural NH₃) that may be associated to traffic NH₃ emissions, as illustrated by the increased correlation with BC ($r=0.60$ between the 21 June and 3 July) (Fig. 6). No similar situation is observed during the rest of the campaign ~~period~~. In Roma, Perrino et al. (2002) ~~have~~ observed high levels of NH₃ at curbside sites with a diurnal profile clearly influenced by traffic emissions. But due to the combined action of dry deposition, dilution after emissions as well as the conversion into particulate NH₄⁺ (with sulfates and/or nitrates), these concentrations were severely reduced at the urban background scale, ~~about a factor of 5~~, and the traffic profile type had disappeared. As a result, our urban background conditions may have prevented us from accurately assessing the potential impact of traffic emissions on ambient NH₃ concentrations. Investigating the NH₃ diurnal variability at the SIRTa site, Petit et al. (2015) noticed a bimodal traffic-like variation but only during spring and not during summer and winter ~~when traffic emissions yet also exist~~, suggesting that these variations may be related to ~~other~~ processes ~~than~~ traffic.

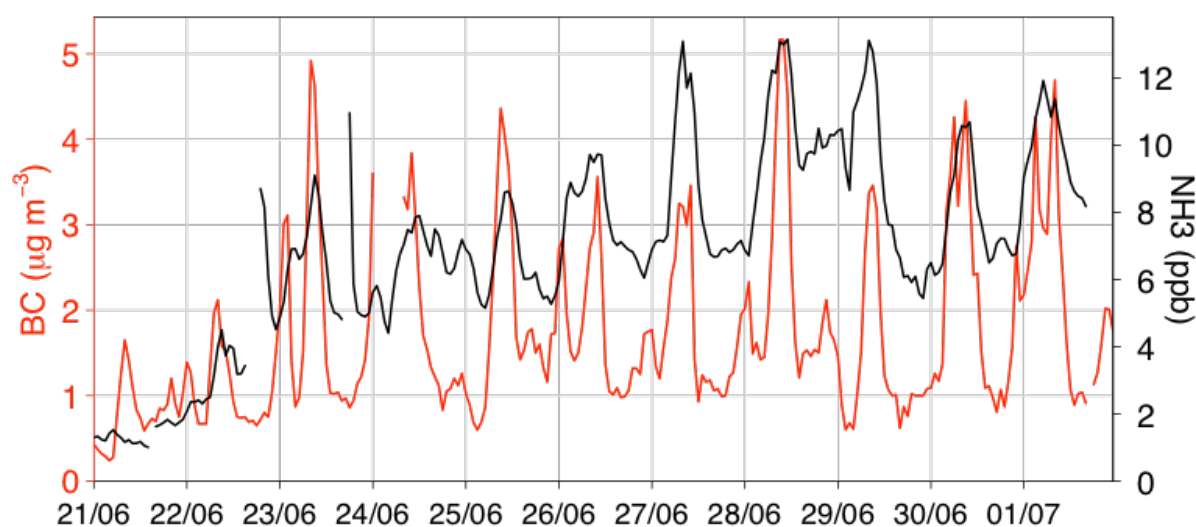


Figure 6: Observed BC (in red) and NH₃ (in black) hourly concentrations at LHVP during the end of June.

4.2.1.3 Influence of agricultural NH₃

As previously mentioned, NH₃ is emitted by both agricultural and non-agricultural sources. The former clearly dominates at the national scale, as well as at the scale of the Paris region (which includes the rural areas surrounding Paris), while the latter ~~obviously~~ dominates at the scale of the city itself (which includes only urban areas). Considering the role of NH₃ in the formation of NH₄NO₃ and the important contribution of this aerosol compound to the PM_{2.5} pollution in Paris, it is of major importance to assess the relative contribution of both types of sources to the NH₃ urban background in the city. Answering that question would ideally require additional NH₃ observations in Paris and its surroundings in order to quantify the increment associated to local sources. Without such observations, it is not possible to quantitatively investigate the NH₃ budget in Paris.

However, based on the available observations, we argue in this section that among all NH₃ emission sources, agriculture is probably the main driver of the day-to-day variability of NH₃ concentrations in Paris during the time of the campaign (from spring to autumn) (in conjunction with the thermodynamic equilibrium that drives the partitioning between the gas and aerosol phases).

This is mainly supported by the NH₃ (and TNH₃) seasonal variations. Although incomplete (due to missing observations in winter and early spring), the NH₃ seasonal pattern shows a maximum in spring and early summer, moderate concentrations in late summer and a minimum in autumn. Such a seasonal pattern has been already reported in several studies (e.g. Reche et al., 2012; Skjøth et al., 2011). A roughly similar variability is expected for the fertilizer applications. Yet this emission source represents around 40% of the total agricultural source at the national scale, and this contribution appears even higher around the Paris region (Hamaoui-Laguel et al., 2014; see in particular their Fig. 2a and 2b). The observed increase of NH₃ with temperature is also compatible with this source, as increased temperature favors fertilizer evaporation (e.g. Hamaoui-Laguel et al., 2014). Conversely, none of the non-agricultural emission sources is expected to be particularly intense ~~at this period~~ of the year. This was discussed for traffic related emissions in the last section. Some NH₃ may also be emitted by biomass burning (for residential heating) but these emissions are, in any case, low in spring and summer. Emissions from sewage and waste disposal as well as emissions from other biological sources may also contribute to NH₃ levels. Interestingly, these latter sources may be influenced by temperature, **as the NH₃ concentrations measured in Paris**. But if they ~~dominant~~, one would not expect ~~so~~ large differences ~~of~~ concentrations between late May, early June and August (when temperatures were comparable). Additionally, in this case, one would also expect higher NH₃ concentrations during stagnant conditions, which is in contradiction with the low correlation between BC and NH₃ (given that such stagnant conditions lead to an accumulation of BC). The NH₃ diurnal profile shows very limited variations along the day, which is consistent with

the idea of a strong NH_3 background originating from agricultural sources around the Paris region. All these elements thus suggest that the agricultural source (and more precisely the fertilizer application) drives a larger part of the NH_3 day-to-day variability in Paris than the other emission sources.

4.2.1.4 Geographical origin of the highest NH_3 episodes

In this section, we investigate the geographical origin of the air masses associated to major NH_3 episodes. Back-trajectories during the 10 days of highest NH_3 concentrations (daily averages above 9.2 ppb, the 95th percentile of all daily values) are presented in Fig. 6a. Most NH_3 episodes are associated to moderate winds in altitude, air masses at D-1 (one day before reaching Paris) being located in a radius of 50-400 km from Paris. A noticeable exception is found on 9 July in the morning (around 6 UTC) when the wind suddenly changes direction (from Southeast to Southwest) and speed (getting much stronger, with air masses originating from Spain at D-1) while NH_3 concentrations increase. Interestingly, some of the highest NH_3 episodes (e.g. 10 July) are associated to oceanic air masses (excepted to be relatively clean) that have spent only a limited time above land, which suggests the presence of intense NH_3 emissions in the corresponding regions (Normandy). As an overall result of this trajectory analysis, air masses with high NH_3 concentrations do not appear to originate from a particular geographical sector. Instead, the highest episodes appear linked to more diffuse NH_3 emissions in the northern part of France, associated to anticyclonic conditions with high temperature and moderate winds. This is in accordance with Petit et al. (2015) that suggest, based on NH_3 measurements at the SIRTa suburban site (south-west of Paris), a diffuse regional NH_3 source, in particular during summer (in spring, some high NH_3 episodes associated to E/NE/SE winds are also noticed, but without any clear pattern).

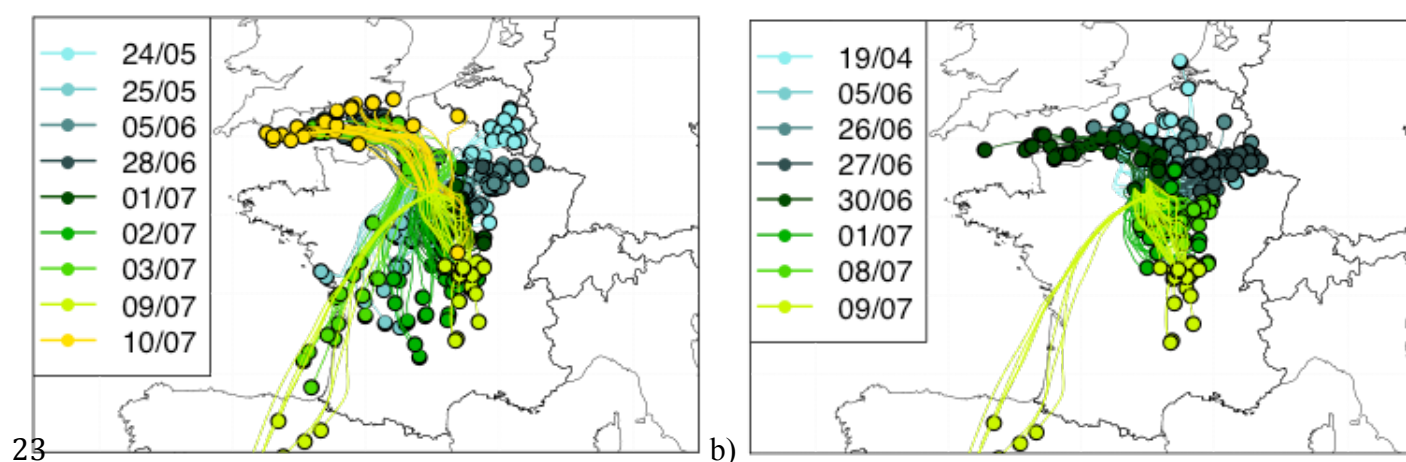


Figure 6: Back-trajectories at D-1 (one day before reaching Paris) associated with highest (a) NH_3 (left panel) and (b) HNO_3 (right panel) episodes (highest episodes being selected according to daily concentrations above the 97th percentile of all daily measurements, i.e. 9.2 and 0.9 ppb for NH_3 and HNO_3 , respectively). For clarity, only back-trajectories of 7 particles around the center of Paris are plotted, each 6 h (i.e. 28 back-trajectories per day).

4.2.2 Model results

As shown in Fig. 2, NH_3 concentrations are significantly underestimated by the CHIMERE model with a NMB of -75% (see statistical results in Table 2). This negative bias not only affects the intense peaks but also the baseline concentrations. In their evaluation of the CALIOPE-EU modelling system, Pay et al. (2012) ~~have~~ reviewed the statistical results of various regional models over Europe (during a whole year for most models). As our study does not cover a whole year, statistical results are not directly comparable, but figures still shed light on the relative performance of our CHIMERE simulation. The negative bias in our study is in the range of those reported from the ~~aforementioned study~~ where NMB spread from -82 to -15 %. Our RMSE (3.9 ppb) is among the best values reported by Pay et al. (2012) (1.6 ppb for the CALIOPE-EU model and 7.6-10.6 ppb for the six other models), as well as the correlation (0.42 ~~against~~ 0.05-0.56). Nevertheless, the CHIMERE model dramatically fails to reproduce the strong spring and summer episodes (and consequently the seasonal variation) during which negative biases on daily concentrations can exceed a factor of 10, despite a monthly distribution of emissions peaking between March and May (spring fertilizer application).

The ~~quite~~ similar results obtained in the MOD and MOD-noIDF cases indicate that most of the simulated NH_3 originates from outside the region of Paris. Concentration maps show that simulated NH_3 concentrations closely follow the spatial distribution of emissions, with maximum levels over Brittany, North of France and Benelux. Due to both dilution and deposition, NH_3 concentrations quickly decrease with distance from these source regions. However, the simulated NH_3 lifetime appears high enough to allow imports over the region of Paris. As an illustration, highest simulated concentrations in the city (4.5 ppb, the 29th April) result from ~~an~~ advection of air masses from Eastern Brittany and South-West during the month of maximum emissions (according to monthly factors applied to emissions).

Comparing observations and model results at the MONTSOURIS meteorological station, ~~we~~ ~~highlighted~~ a negative bias on temperature (-1.6°C) and a positive ~~one on~~ RH (+5.9% in absolute) (see Sect. S.2 in the Supplement). This favors the formation of NH_4^+ and thus decreases gaseous NH_3 in TNH_3 . However, correcting these errors in the ISORROPIA model (i.e. replacing the simulated temperature and RH ~~values by the measurements~~, without modifying TNH_3 , TNO_3 and TS concentrations) does not fill the gap with observations, the average NH_3 concentrations being increased by only 7% on average. Errors may be larger close to the deliquescence point where the influence of RH is stronger. The deliquescent RH (DRH) of NH_4NO_3 and $(\text{NH}_4)_2\text{SO}_4$ at 298K are 61.8 and 79.9%, respectively (Seinfeld and Pandis, 2006). A mixture of both salts will have a DRH between these two extreme values. Focusing on days where RH ranges between 60 and 80% (i.e. close to the deliquescent point of the mixture), the average NH_3 increase is even lower (6%). It

reaches 14% when considering RH between 60 and 65%. In any case, the impact remains limited. As shown in Fig. 5, the fraction of NH_3 in TNH_3 simulated by CHIMERE is highly variable, ranging from less than 5% to about 90%, in contradiction with observations which show a clear gas phase reservoir during spring and summer (at around 60-100%). The already mentioned overestimation of SO_4^{2-} in CHIMERE (see Sect. 4.1) may directly reduce the amount of NH_3 available in the gas phase. However, the bias on TNH_3 is only reduced to -56% (against -76% for NH_3 alone), which indicates that only a minor part of the negative bias on NH_3 can be explained by an erroneous partitioning between both gas and aerosol phases (including errors related to SO_4^{2-}).

Although not likely the main NH_3 source (see Sect. 4.2.1.3), the traffic can also contribute to the NH_3 urban background levels in Paris. Yet in the TNO-MP inventory, these traffic emissions are missing in the Paris region (but not outside this region) (see Table S3 in the Supplement), which may induce an underestimation of modelled NH_3 concentrations. The contribution of traffic to ambient NH_3 levels in urban environments is highly variable from one city to another, as illustrated by the $\text{NH}_3/(\text{NH}_3+\text{NO}_x)$ emission molar ratios that range from a few percent (Yao et al., 2013) to a few tens of percent (Bishop et al., 2010) which are due to differences in the vehicle fleet (Carslaw and Rhys-Tyler, 2013). Several sensitivity tests were performed with added NH_3 traffic emissions, derived from the NO_x traffic emissions with $\text{NH}_3/(\text{NH}_3+\text{NO}_x)$ conversion factors in the range of the values given in the literature : 1, 6, 12 and 18% (not shown). Such additional emissions reduce the bias, but do not improve the correlation between model and measurements. In particular, they induce a clear increase of NH_3 concentrations during the morning and evening rush hours, which is not in agreement with the observed diurnal profile. These results thus prevent us from concluding on the importance of these traffic emissions on NH_3 urban background levels.

A large part of the model errors probably arises from the representation of NH_3 air-surface exchanges (agricultural emissions and deposition) in the CHIMERE model. This representation is by far too simplistic in several respects: (i) the parameterization of NH_3 dry deposition is unidirectional and does not take into account the compensation with emissions; (ii) the agricultural emissions are temporally disaggregated based on monthly, day-of-the-week and diurnal factors without taking into account any environmental factor (e.g. air temperature, soil moisture, agricultural practices) known to influence some NH_3 emissions (e.g. the volatilization of fertilizers). This likely explains the much lower NH_3 -temperature correlation obtained in the model in comparison with observations ($r=0.52$ against 0.72 in observations), as illustrated in Fig. 4. In light of our comparison, the parameterization of the NH_3 emissions in CHIMERE cannot represent the high spatio-temporal variability of NH_3 concentrations, and in particular fails in reproducing the large NH_3 peak values observed during the campaign. Indeed, these emissions result from very complex mechanisms in which numerous environmental parameters are involved, including the

amount of nitrogen fertilizers used over the land; temperature, moisture and pH of the soil; the amount of soluble carbon; the soil disturbance and compaction; fertilization methods (Ma et al., 2010; and references therein). More elaborated parameterizations of NH_3 bi-directional fluxes have been proposed to better handle emission and deposition processes in CTMs (Massad et al., 2010; Zhang et al., 2010; Pleim et al., 2013). Hamaoui-Laguel et al. (2014) have simulated more realistic NH_3 emissions over France during the spring 2007 by combining the one-dimensional mechanistic model VOLT'AIR (Garcia et al., 2011; Générumont and Cellier, 1997) with agricultural practice and soil data. They have shown a spatial variability of NH_3 emissions mainly driven by the soil pH and the types and rates of fertilization, while the temporal variability was rather driven by meteorological conditions and fertilization dates. Compared to the EMEP inventory (quite similar to TNO-MP for NH_3 emissions), the emissions computed with the VOLT'AIR mechanism appear lower over the Brittany (in the West of France) and higher over the North of France (around a factor of 2-3). This would suggest a possible underestimation of agricultural NH_3 emissions close to the Paris region.

Dry deposition of NH_3 and wet deposition of NH_4^+ represent the two major sinks for NH_3 and NH_4^+ , respectively; the first being dominant near emission sources whereas the second dominates at a larger scale (Asman et al., 1998). Uncertainties in the parameterization of both dry and wet deposition in the CHIMERE model may also partly explain the NH_3 underestimation. Results from the MOD-noddep sensitivity test (with no NH_3 dry deposition) allow assessing an upper bound of uncertainties related to dry deposition. On average, more than half of the NH_3 reaching Paris is deposited in the MOD case, as illustrated by the increase of NH_3 concentrations by a factor of 2.2 when deposition is removed. The diurnal profile indicates that deposition in CHIMERE more strongly affects night-time concentrations, likely due to the shallow boundary layer. Daytime concentrations are also affected but approximately 2 times less than night-time ones. Note that typical deposition velocities simulated by CHIMERE are around 0.3 cm s^{-1} , although it can substantially vary in time and space. Despite the unrealistic character of this sensitivity test (dry deposition being one of the dominant NH_3 sinks), this appears not sufficient to increase concentrations towards observed ambient levels (NMB of -46%). Thus, deposition does not appear as the major source of error in the CHIMERE simulated NH_3 .

4.2.3 Conclusions on ammonia

Our NH_3 urban background measurements in Paris have highlighted several intense episodes in late spring and early summer. These episodes occur during anticyclonic conditions with high temperature, expected high agricultural emissions and moderate winds enabling an accumulation of NH_3 and a subsequent advection over the city. We argued that the observed NH_3 seasonal pattern

supports the idea of a NH_3 day-to-day variability mainly driven by the agricultural source, in association with the thermodynamic equilibrium controlling the gas-aerosol partitioning. CHIMERE simulations show a significant negative bias on NH_3 , both for the baseline concentrations and the intense episodes. Errors in the partitioning of TNH_3 between the gas and aerosol phases (due to errors in modelled SO_4^{2-} , NO_3^- or local meteorology) as well as uncertainties on deposition can only explain a minor part of the bias. Thus, the simulated NH_3 concentrations appear mainly affected by uncertainties in emissions, and in particular the lack of dynamical treatment of agricultural emissions as a function of environmental factors (temperature, etc.) in the CHIMERE model (the annual total emissions being simply disaggregated with a monthly profile).

4.3 Nitric acid

4.3.1 Temporal variability

Daily concentrations and the diurnal profile of HNO_3 are shown in Fig. 2. Over the whole period, the average HNO_3 concentration is 0.25 ppb. Several moderate episodes are observed in spring and early summer, with daily concentrations up to 1.2 ppb at the beginning of July. This leads to a seasonal pattern characterized by higher values in spring/summer compared to autumn/winter. Such temporal variations are expected in urban environments close to NO_x emissions due to both the higher OH triggered HNO_3 production in summer and the higher temperatures (as well as the lower RH) that diminish its condensation into particulate NO_3^- . They are also consistent with those found in other urban studies (Cadle et al., 1982 and Cadle, 1985 in Warren, Michigan, United-States (US); Solomon et al., 1992 in Los Angeles, California, US; Perrino et al., 2002 in Roma, Italy).

In Paris, the highest HNO_3 episodes are associated with high temperatures and low-to-moderate wind speeds at ground. These conditions increase the atmospheric stratification and the residence time of NO_x emissions over the agglomeration and allow for a more efficient HNO_3 formation via the $\text{NO}_2 + \text{OH}$ reaction. This is confirmed by the fact that many HNO_3 peaks follow BC episodes, these episodes being most of time due to stagnant conditions allowing the accumulation of the BC emitted by the traffic.

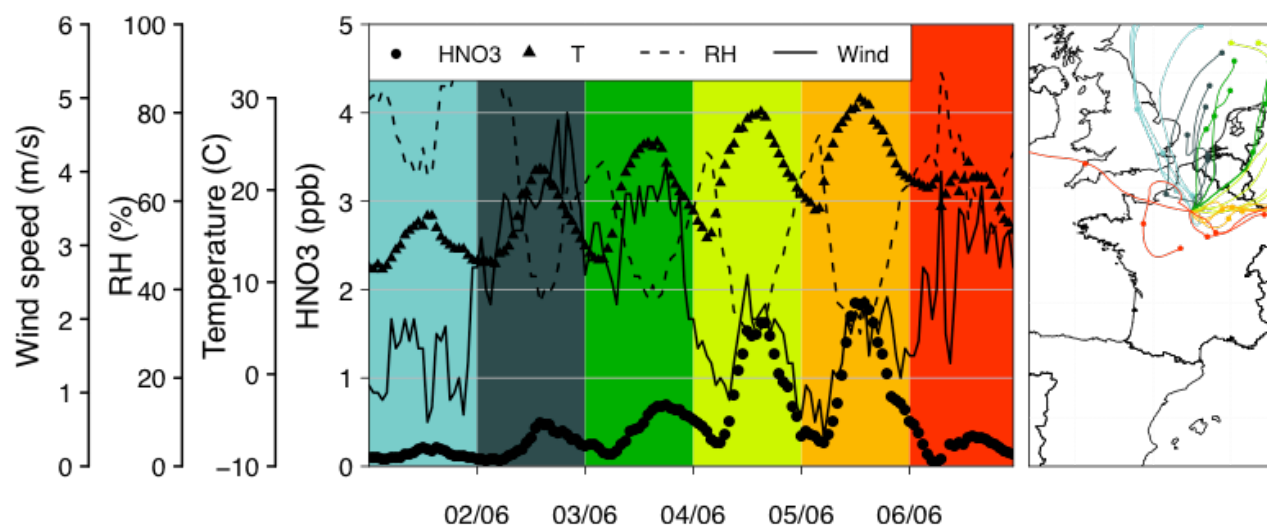


Figure 8: Hourly concentrations of HNO_3 at LHVP and wind speed, RH and temperature during early June 2010 (left panel), and associated 48h back-trajectories (one point every 24h) coloured by the day of arrival (i.e. red is for 06/06).

This is illustrated during the first days of June in Fig. 8. The 1st of June is characterized by low wind speed but cloudy conditions that decrease the photooxidation rate of NO_x . During the next 2 days, stronger wind-speed (above 3 m s^{-1}) and increasing temperatures are observed, associated to a moderate increase of HNO_3 concentrations. A much higher increase of HNO_3 concentrations is observed the 4th and 5th of June concomitantly with high temperatures (up to 30°C) and slow winds. Such stagnant conditions during the night allow the accumulation of NO_2 , as shown by the NO_2 measurements at an AIRPARIF station located right next to the LHVP site (not shown). In the early morning of the 4th (5th) of June, NO_2 concentrations reach 83 (110) ppb, and fall below 20 ppb during the afternoon. As for NH_3 , no additional HNO_3 measurements are available upwind of Paris, which prevents us from quantitatively assessing the importance of local formation versus imports. But this specific situation of early June supports the idea of a strong local formation of HNO_3 . Some HNO_3 is also probably (slowly) advected by north-easterly winds but the strong photochemically driven diurnal variation observed during these days (where concentrations reach 1.5 ppb in the afternoon) suggests that this contribution is minor in comparison to the local formation. The episode ends concomitantly with a significant decrease of temperature and more dispersive conditions.

The diurnal profile shows maximum HNO_3 concentrations in the afternoon at around 14:00-18:00 UTC (Fig. 2). On average, the ratio between daytime and nighttime HNO_3 concentrations is close to a factor of 2 (despite the development of the convective boundary layer in the afternoon). A slight decrease of HNO_3 is found at around 6:00 UTC, which may be explained by dew formation processes that allows the absorption of water-soluble gases such as HNO_3 (Mulawa et al., 1986; Parmar et al., 2001; Pierson et al., 1988).

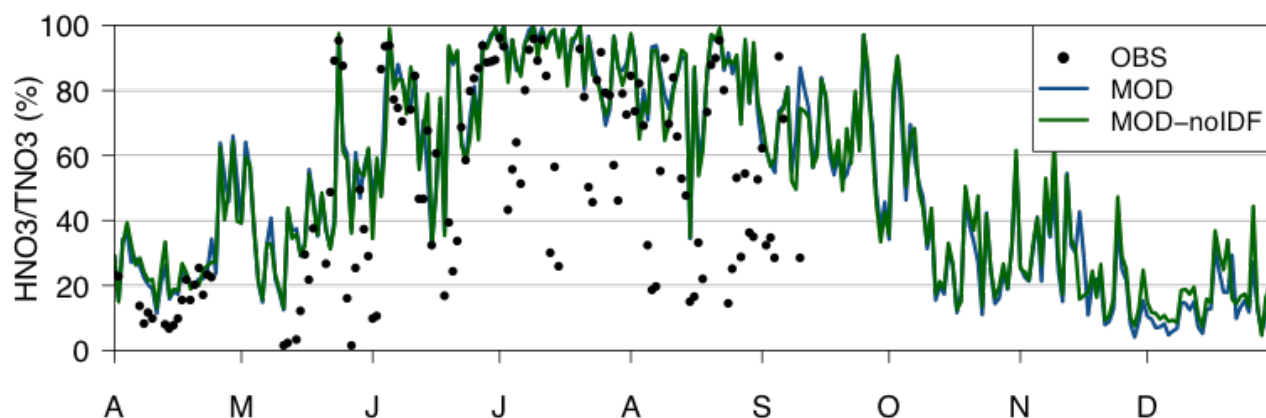


Figure 9: Daily $\text{HNO}_3/\text{TNO}_3$ ratios.

HNO_3 accounts for 51% of TNO_3 on average (Fig. 9) but this fraction appears highly variable. The lowest $\text{HNO}_3/\text{TNO}_3$ ratios (a few %) are observed during cold days in mid-May when daily temperatures fall below 8°C (see Fig. S2 in the Supplement), while the highest ratios occur during early summer, with values up to 96%. The correlation between the $\text{HNO}_3/\text{TNO}_3$ ratio and the temperature is 0.82, which illustrates the impact of temperature on the thermodynamic equilibrium. Despite rather high temperatures, low ratios (below 40%) are also observed on specific periods during summer, particularly in August. Such a pattern may be due to higher measurement uncertainties occurring for low TNO_3 concentrations, closer to the detection limit (roughly around 0.1 ppb for HNO_3). In August, ratio values below 40% indeed correspond to HNO_3 and TNO_3 concentrations below 0.2 and 0.7 ppb, respectively.

4.3.2 Model results

HNO_3 concentrations are significantly overestimated by CHIMERE, with a NMB of +195%, leading to a large error (NRMSE of 320%), in particular at mid-day where the bias can reach a factor of 4 (as illustrated by the diurnal profile in Fig. 2). The correlation is moderate ($r=0.56$) when considering hourly concentrations, but is slightly higher with daily values ($r=0.68$).

Several uncertainties may explain the discrepancies between observed and simulated HNO_3 concentrations: (i) uncertainties in NO_x emissions at both local and regional scales, (ii) uncertainties in the thermodynamic equilibrium (i.e. the errors on either the other inorganic compounds or the ISORROPIA model itself) that determine the distribution between gas and aerosol phases, (iii) uncertainties in the OH concentrations that directly influence the conversion of NO_2 into HNO_3 , (iv) uncertainties on the HNO_3 deposition, and (v) errors in the transport. At the European scale, uncertainties on NO_x emissions are estimated to be around 30% (Deguillaume et al., 2007; Konovalov et al., 2006) and are thus much lower than the errors obtained for modelled HNO_3 . Over the Paris agglomeration, NO_x emissions from the TNO-MP inventory used in our model have been evaluated during the summer 2009 based on aircraft measurements in the Paris plume, showing no significant bias (Petetin et al., 2014). Dry deposition plays an important role in the HNO_3 budget,

and corresponding parameterizations incorporated in the CHIMERE model have been poorly evaluated so far. In fact, a too low deposition rate modelled by CHIMERE may partly explain the positive bias on HNO_3 . In CHIMERE, HNO_3 deposition velocities are typically below 1.5 cm s^{-1} , which appears on the lower end of the values reported in the literature (Brook et al., 1999). However, due to a lack of appropriate data, this hypothesis remains difficult to assess. Finally, important errors on the transport pattern remain unlikely given the good correlations obtained on nitrates between the observations and the model. The next subsections aim to investigate in more details the uncertainties related to the simulated thermodynamic equilibrium and OH radical.

4.3.2.1 Uncertainties associated with thermodynamic equilibrium

Bias and RMSE are much lower for TNO_3 (NMB of +71%, NRMSE of 121%) than for HNO_3 , because the CHIMERE model overestimates the $\text{HNO}_3/\text{TNO}_3$ fraction (on average 68% for the model against 51% observed from experimental data during the period with available observations of NO_3^- and HNO_3). Partitioning errors may derive from uncertainties in the ISORROPIA thermodynamic model (e.g. model formulation, chemical compounds included, activity coefficients treatment) or in its input data. Apart from CHIMERE, the ISORROPIA model is used in many other CTMs, including LOTOS-EUROS (Schaap et al., 2008), REM-CALGRID (Stern, 2003), CAMx, FARM or CMAQ. It has been validated in various studies based on comparisons with observations (Moya et al., 2001) or against other widely used thermodynamic models (Nenes et al., 1999; Carnevale et al., 2012). From these studies, several uncertainty sources emerge: The hypothesis (used in ISORROPIA) of an instantaneous equilibrium between gas and aerosol phases (Aan de Brugh et al., 2012) is without incidence for our study, since the CHIMERE model treats the evolution of inorganic compounds concentrations through a dynamic approach (see Sect. 3.1). The absence of sodium, chloride and other crustal species (Ca^{2+} , K^+ , Mg^{2+}) in our simulations may also induce errors in the system (Fountoukis and Nenes, 2007), but the contribution of this crustal material remains low in the Paris region, about 5% on average from 1 April to 10 September (with a percentile 95 at 13%), as previously noted by Bressi et al. (2013). This low contribution of crustal species is confirmed by the ion balance obtained by considering only ammonium, nitrate and sulfate: NH_4^+ versus $\text{NO}_3^- + 2\text{SO}_4^{2-}$ (all species expressed in neq m^{-3}) gives a slope of 1.01, an y-intercept of -0.20 and a correlation $r^2=0.97$ (see Fig. S1 in the Supplement).

Therefore, errors in the modelled partitioning are most likely due to errors in the other inorganic compounds involved in the $\text{HNO}_3\text{-NO}_3^-$ equilibrium. In particular, the large negative bias on NH_3 described in Sect. 4.2 can potentially lead to an underestimation of the NH_4NO_3 formation and consequently to an overestimation of HNO_3 . A sensitivity test has been performed for that purpose with the ISORROPIA model running alone (i.e. not coupled with CHIMERE) fed by the concentrations previously obtained with CHIMERE for inorganic species except for NH_3 for which

measurements were taken into account. This approach changes HNO_3 concentrations, ~~with~~ for instance a decrease of 29% in May. However, the significant positive bias in HNO_3 in summer persists (HNO_3 concentrations decrease by only 11% between June and August), mainly because during summer, ~~due to high temperatures,~~ NH_4NO_3 is very weak and HNO_3 is the major TNO_3 component.

4.3.2.2 Uncertainties associated with OH concentrations

Assuming that (i) the $\text{NO}_2 + \text{OH}$ reaction is likely the dominant direct homogeneous pathway for HNO_3 formation during the summertime period, (ii) a significant bias is observed for modelled TNO_3 , and (iii) the maximum discrepancies between measurements and modelled HNO_3 are found during mid-day, uncertainties on simulated OH could explain a substantial part of the errors on HNO_3 . Many studies have attempted to quantify uncertainties on sources and sinks of OH, traditionally through the direct comparison between observations and calculations from detailed chemistry schemes (in box models) fed by ancillary observations of various parameters (e.g. VOC, NO_x and O_3 concentrations, photolysis rates). In such exercises, uncertainties in daytime OH concentrations usually remain below a factor of 2 (see Kanaya et al. (2007) for a review, where simulated over observed OH daytime concentrations ratios range between 0.5 and 1.5). During summertime, Michoud et al. (2012) have shown in Paris a very low overestimation (5%) of OH concentrations simulated with the Master Chemical Mechanism (MCM) chemistry scheme. However, these results need to be taken as a lower end of OH uncertainties in CTMs where constraints are neither applied on long-lived compounds nor on photolysis rates. This is especially true in an urban environment where concentration gradients of compounds impacting on the OH budget are strong.

In order to assess the influence of OH on HNO_3 formation, a sensitivity test (hereafter designated by MOD-OHx0.5) has been performed (~~over a period of 35 days in June/early July~~) by artificially reducing OH concentrations. This is technically performed by decreasing by a factor of 2 the HO_x ($\text{HO}_x = \text{OH} + \text{HO}_2 + \text{RO}_2$) formation yields (i.e. the stoichiometric coefficient) in several (initiation) reactions, including the photolytic destruction of ozone, formaldehyde, acetaldehyde, glyoxal and methyl glyoxal. OH and HNO_3 concentrations are then compared with the reference MOD case in Fig. 10. On average, concentrations of OH and HNO_3 are reduced by -36 and -16%, respectively. The changes in NO_x concentrations remain below 3%, which means that only a minor fraction of NO_x is oxidized within Paris. These decreases are even more important during mid-day where they reach -42 and -25%, respectively. Over mid-day, the bias between measured and modelled HNO_3 is reduced and equals to +113% (against +154% in the MOD case). Uncertainties in the OH radical may thus explain a significant part of the CHIMERE errors on HNO_3 .

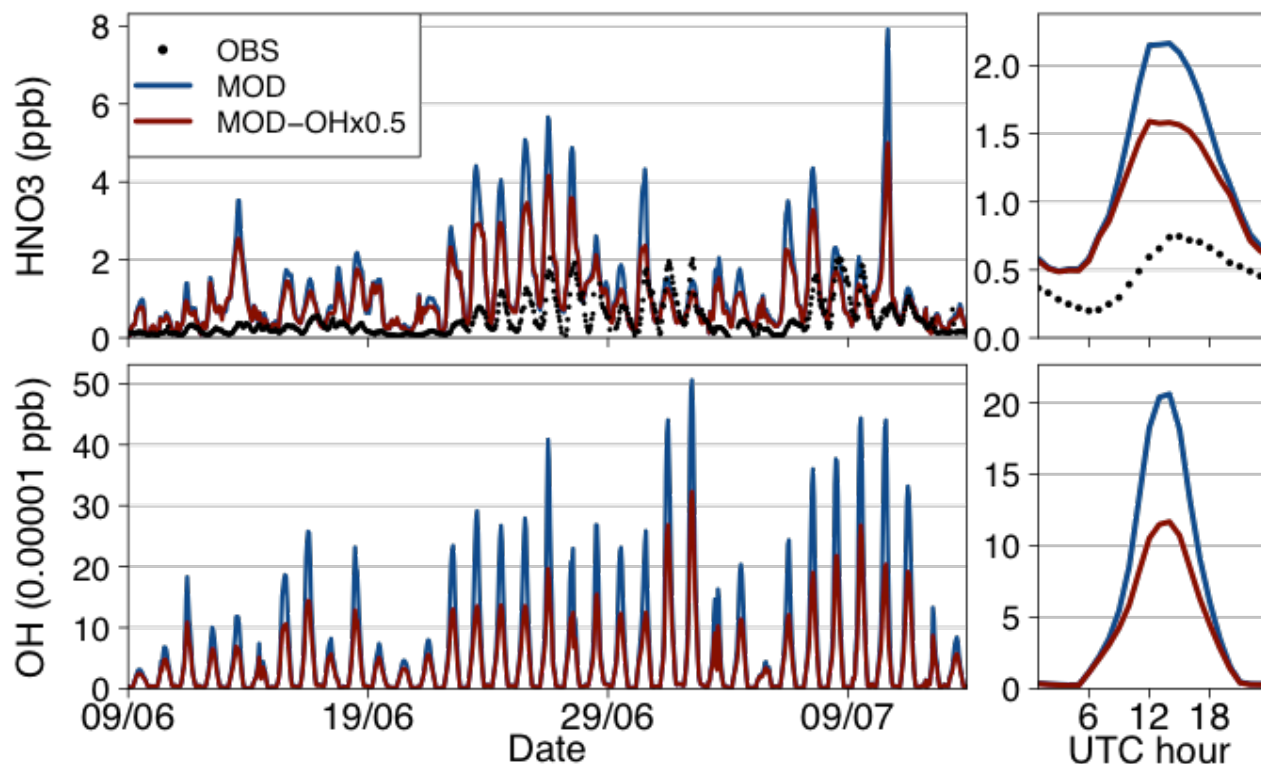


Figure 10: HNO_3 and OH hourly concentrations (left panel) and diurnal profiles (right panel) at the LHVP site.

4.3.3 Conclusions on HNO_3

HNO_3 concentrations experimentally determined in Paris show several intense peaks in late spring and early summer that coincide with high air temperatures and low to moderate winds. The share between local production and imports remains difficult to assess precisely, but local HNO_3 may represent a major source on some specific time-limited episodes. However, uncertainties persist, and the CHIMERE errors are unfortunately too high to help the investigation of HNO_3 origin. Indeed, the model largely overestimates measured HNO_3 concentrations, approximately by a factor 3, with the highest biases observed in the middle of the day. The negative bias between measured and modelled NH_3 explains a part of the poor model performance for HNO_3 , but still fails to explain errors during summertime when TNO_3 is mostly in the gas phase. Uncertainties on NO_x emissions are much lower than errors obtained on HNO_3 and cannot explain the results of the model. Uncertainties related to the dry deposition of HNO_3 cannot be assessed and could contribute to the discrepancies given by the model. Finally, a too strong NO_2 -to- HNO_3 conversion through an overestimation of the OH radical concentrations in CHIMERE could also contribute to the large modelled overestimation of HNO_3 formation. Indeed, uncertainties on simulated OH remain still high in CTMs, probably more than a factor of 2, and reducing OH sources have shown to lead to a significant decrease of OH and HNO_3 concentrations, in particular during the afternoon when NO_2 photooxidation (as well as the HNO_3 bias) is at its maximum.

4.4 Aerosol Nitrate formation

4.4.1 Results of the CHIMERE simulations

Fine particulate pollution with high nitrate contents in Paris consists in intense (up to $16 \mu\text{g m}^{-3}$ in late spring) and time-limited (a few days) episodes associated with continental wind regimes. Very low levels of nitrate are observed during periods with marine (clean) air masses and during summertime (due to volatilization). Despite the large errors previously highlighted for both NH_3 and HNO_3 , the CHIMERE model provides quite satisfactory results for nitrate with a NMB of +19% and a correlation of 0.81, but still with a large NRMSE (109%). As previously mentioned, in the framework of the PARTICULES campaign, $\text{PM}_{2.5}$ chemical constituents have also been measured at 3 rural sites all around the Paris region. Results have been analyzed in terms of local and imported contributions by Petetin et al. (2014). In a few words, concerning sulfates, imports were slightly underestimated by CHIMERE (-17%) while the (low) local production was overestimated (+32%), leading at the end to a moderate negative bias (-17%). For nitrates, a similar but stronger error compensation was underlined between imports and local production (bias of +63 and -109%, respectively), leading to a reasonable bias on concentrations in Paris (+23%). For more details, the reader is invited to look at this previous paper (e.g. statistical results in Table 7).

It is worth noting that the positive bias highlighted here on the urban background concentrations in Paris should partly originate from experimental (negative) artifacts. Actually, the model may underestimate NO_3^- if the experimental data are corrected for semi-volatile losses. The semi-volatile particulate matter (SVPM) can be deduced from the difference between TEOM-FDMS and TEOM $\text{PM}_{2.5}$ concentrations. If we attribute all that SVPM to NH_4NO_3 , the bias between measured and modelled NO_3^- becomes -48%. This corresponds to an upper bound of the bias since SVPM not only contains NH_4NO_3 but also semi-volatile OA. And actually, semi-volatile OA may contribute the most to SVPM, as suggested by the higher correlation of SVPM with OA in comparison with NH_4NO_3 (0.59 against 0.32).

As a conclusion, the either positive or negative bias on simulated nitrates and ammonium remains relatively small in comparison with the biases reported previously for precursor species. Such a result is not intuitive, and cannot be trivially explained. An interesting point to illustrate the possible error compensations concerns the saturation condition that needs to be achieved to allow the formation of nitrates. This condition is defined as (Ansari and Pandis, 1998):

$$[\text{TNO}_3]([\text{TNH}_3] - 2[\text{TS}]) > K \quad (6)$$

with K the equilibrium constant that depends on various parameters, including temperature and RH. It is obvious here that the errors on TNO_3 and TNH_3 can thus (partly) compensate each other. On average, the left-hand term is 3.6 and 2.5 ppb^2 based on observations and simulation, respectively. It corresponds to a NMB of -31%, thus much lower than the NMB affecting the different species

(+71%, -56% and +48% for TNO_3 , TNH_3 and TS). This result thus suggests that the formation of nitrates is slightly more difficult in the model than in the reality, which would be consistent with a moderate negative bias on nitrates. Due to the possible artefacts, our dataset does not allow a complete assessment of the nitrate formation. It would be useful in the near future to evaluate the CHIMERE model with artefact-free measurements (for instance with aerosol mass spectrometer (AMS) or aerosol chemical speciation monitor (ACSM)).

4.4.2 Gas Ratio and limiting species for nitrate formation

The Gas Ratio (GR) has been proposed to assess which species among NH_3 and HNO_3 is the limiting reactant for NH_4NO_3 formation (Ansari and Pandis, 1998). It is defined as follows (with concentrations expressed in ppb):

$$GR = \frac{[\text{TNH}_3] - 2[\text{TS}]}{[\text{TNO}_3]} \quad (7)$$

GR values above 1 indicate a regime mainly limited by nitric acid (i.e. NH_3 -rich regime) in which there is enough NH_3 to neutralize both sulfate and nitrate. Conversely, a GR between 0 and 1 indicates that there is enough NH_3 to neutralize sulfate but not nitrate, while negative GR corresponds to a NH_3 -poor regime in which NH_3 amounts are insufficient to even neutralize sulfate. Non-linear PM responses to inorganic concentration changes are expected at GR near unity (Ansari and Pandis, 1998).

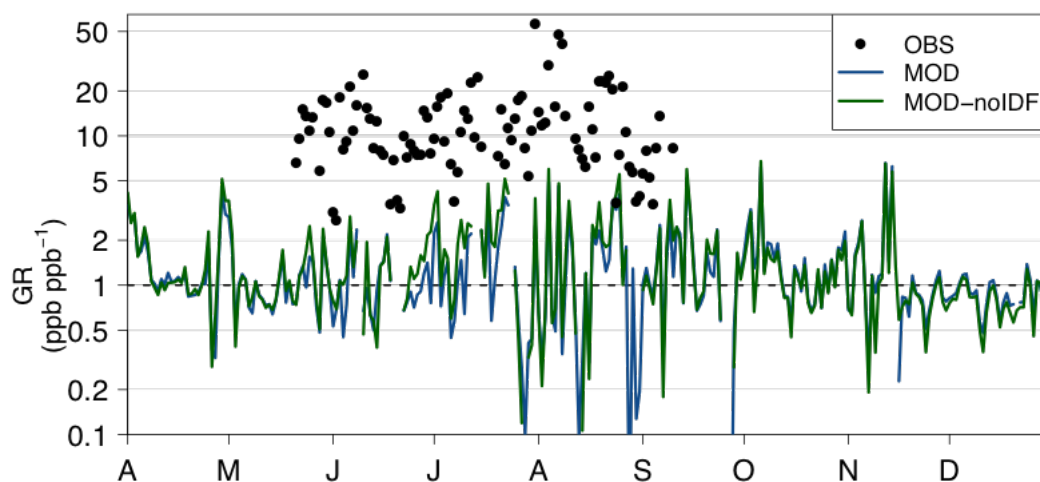


Figure 12: Observed and modelled daily GR.

As shown on Fig. 12, daily GR measurements are available only from the end of May (no NH_3 observations before) until the beginning of September (no aerosol observations after). During that period, experimentally determined daily GR values are highly variable (ranging between 2.8 to 56.3) but always remain above unity (12.6 on average), thus indicating that a large amount of ammonia is available for neutralizing nitric acid.

Observed GR may be affected due to the negative artefacts of nitrate filter measurements (Sect. 2.1). If we assume here that all the SVPM is NH_4NO_3 (see Sect. 4.4.1), one can calculate an

artefact-corrected GR with both evaporated NH_4^+ and NO_3^- added to measured TNH_3 and TNO_3 , respectively. Compared to the previous GR, the artefact-corrected GR is reduced to an average value of 7.3 (the median is 3.5), thus still well above 1. In addition, as noticeable amounts of OA are expected to be included in the evaporated part, this artefact-corrected GR has to be considered as a lower estimate of the actual GR values. The nitrate formation in Paris thus appears mainly limited by HNO_3 . Over Europe, Pay et al. (2012) have also observed GR above 1 in several regions (e.g. Switzerland, Italy, Austria, inland regions of Spain and Denmark; no data in France), but taking into account observations restricted to regional background stations (i.e. enriched by agriculture (NH_3) emissions instead of traffic (NO_x) emissions). In our study, we show that such a NH_3 -rich regime is also observed within a large megacity like Paris. Considering the high NO_x emissions in the Paris megacity, such a result is very interesting, but could likely be explained, as previously mentioned in Sect. 4.3.2, by a too slow NO_x -to- HNO_3 conversion rate compared to the efficient dispersive conditions.

In the CHIMERE model, the negative bias on TNH_3 and the positive ones on TNO_3 and SO_4^{2-} concur of all them to a significant underestimation of modelled GR. On average, the model simulates a GR slightly above unity (1.2). Daily values continuously alternate between both regimes with, over the period with available observations data (100 days), 48% of simulated daily values remaining below unity (47% considering the whole dataset). The dataset does not show any period with specific (and permanent) pattern for GR. Actually, the diurnal profile given by CHIMERE indicates that the regime changes within a single day, the lowest GR values (below 1) being simulated at 12:00 UTC (between the maximum TNO_3 occurring at 8:00 UTC and the minimum TNH_3 simulated at 15:00 UTC). Therefore, due to significant errors in gaseous precursors (and to a lesser extent in sulfate), the CHIMERE model fails half of time at retrieving correctly the HNO_3 -limited regime for nitrate formation in Paris on a daily basis.

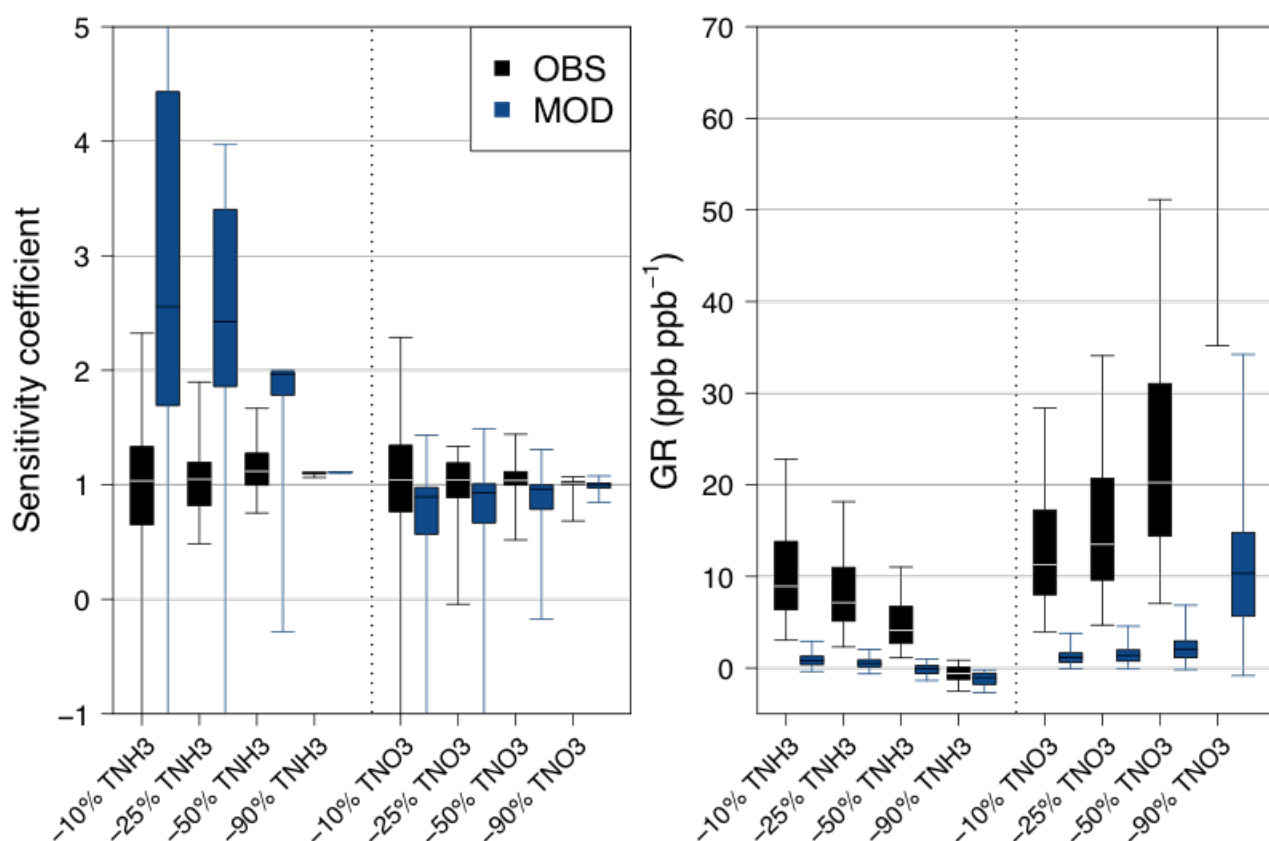
4.4.3 Sensitivity to perturbations

The GR value alone does not allow predicting the sensitivity of nitrate formation with respect to changes in gas precursors concentrations. This is due to the inability of GR to take into account neither the need for the atmosphere to be saturated with NH_3 and HNO_3 (which acts as a threshold effect, see formula 6 in Sect. 4.4.1), nor the influence of temperature and RH. Additional information can be given by the sensitivity coefficient S_x (Takahama et al., 2004) of nitrate formation, defined as:

$$S_x = \frac{\Delta \text{NO}_3}{\text{NO}_3} \frac{x}{\Delta x} \quad (8)$$

where ΔNO_3 refers to the change in nitrate concentrations obtained after a Δx change of the parameter x (e.g. temperature, RH, TNH_3 , TNO_3 or TS).

1 The ISORROPIA thermodynamic model is used here to compute this sensitivity coefficient S_x as a
2 function of various decreases (-10, -25, -50 and -90%) in TNH_3 and TNO_3 concentrations. This 0-
3 dimension model requires five inputs – temperature, RH, and TNO_3 , TNH_3 and TS concentrations
4 – and computes the gas-aerosol partitioning coefficient of both TNO_3 and TNH_3 compounds. Also
5 note that the analysis is local, it is performed for the observed and simulated set of parameters at the
6 urban background site. Decreasing the concentration of a family species – TNO_3 or TNH_3 in our
7 case – leads to a change in its partitioning between both gaseous and aerosol phases. This change
8 not only depends on the concentration of the family species which is altered but also on the value of
9 all the other parameters of the system. Thus, the CHIMERE errors in the different input parameters
10 propagate to the gas-aerosol partitioning coefficient, which can potentially lead to an erroneous
11 sensitivity of nitrates to a change of TNO_3 or TNH_3 . Calculations are performed for both the
12 measurements and the model, i.e. all inputs are taken from the observations and the model,
13 respectively, at the urban background site. In each case, the (observed or simulated) concentrations
14 of TNH_3 or TNO_3 are decreased and the sensitivity coefficient is computed to quantify the impact of
15 this change on the nitrate concentrations. Sensitivity coefficient results and corresponding GR are
16 shown as box-plots in Fig. 13.



17
18 Figure 13: Sensitivity coefficient S_x of nitrate formation due to different changes (-10, -25, -50 and -
19 90%) in TNH_3 and TNO_3 concentrations (left panel) and resulting GR (right panel) during the
20 period from 15 May to 10 September 2010. Experimental data (OBS) in black, modelled data
21 (MOD) in blue. Box plots indicate 5th, 25th, 50th, 75th and 95th percentiles.

For the experimental data, we do observe a quite similar sensitivity of nitrate formation for changes either in TNH_3 or in TNO_3 concentrations, with median sensitivity coefficients around 1 (i.e. close to a linear response). Considering the high GR values (except for the -50 and -90% TNH_3 cases that lead to negative GR), such a result with similar responses to both precursors changes appears quite counter-intuitive in light of the above definition of GR. However, first, the GR approach considers free NH_3 , while the sensitivities are calculated with respect to total NH_3 . Second, as already mentioned, the formation of nitrates requires the saturation condition to be achieved (see formula 6). So for large GR values, but small TNO_3 and free NH_3 values, nitrate formation will be sensitive to both TNO_3 and TNH_3 . Note that the equilibrium constant K (and thus the nitrate sensitivity) also depends on temperature and RH; this is illustrated in Fig. S6 in the Supplement where the same sensitivity tests are performed after decreasing the temperature by 10°C and increasing the RH by 0.20 in observations, which leads to S_{TNO_3} (still close to 1) much higher than S_{TNH_3} (below 0.5 for -10 and -25% of TNH_3), in accordance with the NH_3 -rich regime given by GR.

The CHIMERE nitrate response to TNO_3 changes is approximately linear (i.e. S_{TNO_3} close to 1), in reasonable agreement with observations. However, the model highly overestimates the sensitivity to TNH_3 changes, with median S_{TNH_3} up to 2.5 for moderate NH_3 decreases while observations show a similar response than for TNO_3 changes (S_{TNH_3} around 1). The model manages to match the observed response only when nitrate formation is severely NH_3 limited (negative GR) and when the aerosol nitrate formation is prevented (which corresponds to the -90% TNH_3 case).

These results have serious implications on the use of the CHIMERE model for emissions reduction scenarios. As TNH_3 concentrations are closely linked to NH_3 emissions, they show that the benefits (in terms of fine aerosol concentrations) of reducing these emissions would likely be overestimated by the model, in particular for moderate reductions (below -50%). In addition, in terms of dynamical evaluation, changes in NH_3 emissions in the next years may potentially degrade the CHIMERE performance on the simulation of NH_4NO_3 in Paris if the issues raised here are not solved. This is an important conclusion for the use of the CHIMERE model (in that configuration and input data) and probably other CTMs sharing similar input data and/or parameterizations.

5 Conclusions

Ammonium nitrate is a major contributor to the fine particulate pollution in Europe, and a better characterization of its formation regime and variability (controlled by the availability of its gaseous precursors, NH_3 and HNO_3) is thus mandatory for setting up relevant PM control strategies.

In this study, long term measurements of inorganic compounds in both gaseous (NH_3 , HNO_3 , SO_2) and aerosol (NH_4^+ , NO_3^- , SO_4^{2-}) fractions have been used to assess the NO_3^- formation regime in the Paris megacity over several months covering the spring/summer period. High episodes of NH_3 (up

to 12 ppb on daily average) were observed during late spring and early summer. Considering both the seasonal and diurnal variations, these observations suggest that agricultural activities are a major driver of the NH_3 day-to-day variability within the Paris megacity. Rather low HNO_3 concentrations were measured (below 1.5 ppb on daily average), despite the large amounts of gas precursors (NO_x) emitted by the traffic in the city of Paris. Some ~~strong~~ HNO_3 episodes ~~are~~ observed during anticyclonic conditions (high temperature, low-to-moderate wind) and suggest a substantial local formation from the NO_x emitted within Paris. However, our dataset does not allow quantitatively assessing the relative contributions of this local formation as compared to imports. These experimental results lead to a NH_3 -rich regime in the Paris urban environment (as indicated by high ~~gas-ratio~~ values), as already observed in previous studies over Europe but only in rural areas (i.e. closer to agricultural activities). However, sensitivity tests with the ISORROPIA thermodynamic model indicate that, in the specific environment of Paris (in terms of RH, temperature and inorganic compounds concentrations), the NO_3^- formation remains ~~quite~~ equally influenced by decreases of TNH_3 and TNO_3 . Considering the size of the Paris megacity and the intensity of NO_x emissions, one would have primarily expected higher HNO_3 and lower NH_3 in the Paris center. This work thus sheds a new light on the topical debate relative to the respective responsibility of traffic and agriculture in the formation of NH_4NO_3 , by highlighting substantial amounts of agricultural NH_3 and relatively low concentrations of HNO_3 in the city.

This detailed experimental dataset has also offered the opportunity to evaluate for the first time the ability of the CHIMERE chemistry-transport model to simulate the NH_3 - HNO_3 - NO_3^- system. Comparison between measurements and model ~~have~~ shown significant negative (-75%) and positive (+195%) biases for NH_3 and HNO_3 , respectively. Several sensitivity tests have been performed in order to rank ~~uncertainty~~ sources ~~being~~ responsible for these ~~important~~ biases. The difficulty of the CHIMERE model to match NH_3 observations is likely ~~mainly~~ due to erroneous agricultural emissions (in particular their spatio-temporal variability). By comparison, the contribution of NH_3 traffic emissions in the Paris agglomeration appears ~~as~~ minor during the studied period but requires a more detailed quantification. Besides the (hardly quantifiable) uncertainties associated with dry deposition, errors ~~on~~ HNO_3 can probably be explained by the large uncertainties ~~on~~ OH concentrations, in particular during summertime while the negative bias ~~on~~ NH_3 explains a noticeable ~~part~~ of the HNO_3 overestimation during spring (by preventing HNO_3 ~~to be converted into~~ NO_3^-).

~~Many studies have evaluated the ability of CTMs to simulate inorganic aerosol compounds, but few have evaluated their performances on gaseous precursors. The low performing modelled results on HNO_3 and NH_3 found here may also exist in other CTMs sharing similar emissions data and/or parameterizations.~~ The sensitivity of NO_3^- formation as a function of decreasing concentrations of

gas precursor have been investigated, highlighting a very high sensitivity to NH_3 changes in the model, in disagreement with observations that give a quasi linear response. Such results may have important implications on the use of CHIMERE for emission reduction scenarios (at least in the Paris region) by potentially overestimating the ~~potential~~ benefit of NH_3 emission reductions in terms of PM concentrations. The diagnostic evaluation led in this paper gives first results that need to be extended, notably with hourly artefact-free (NH_4NO_3) measurements during all seasons, in order to assess more precisely the NO_3^- formation regime in the city of Paris. Additional work on uncertainty sources is also required to reduce the highlighted errors, in particular the NH_3 agricultural emissions and the OH uncertainties. ~~In that perspectives,~~ the recent NH_3 measurements provided by IASI (Infrared Atmospheric Sounding Interferometer; Clarisse et al., 2009, 2010) may offer opportunities to better assess the spatial distribution of NH_3 emissions and help building more accurate emission inventories.

Acknowledgements

This work is funded by a PhD DIM (*domaine d'intérêt majeur*) grant from the Ile-de-France region. The PARTICULES project has been funded by the French state, the Ile-de-France region and the Paris city. The FRANCIPOL projet has received funding from PRIMEQUAL, CNRS, CEA, the Ile-de-France region, ACTRIS and DIM R2DS. The authors gratefully acknowledge Jean-Charles Dupont and the SIRTa (sirta.ipsl.fr) for the useful boundary layer height data. The other meteorological data at Montsouris site have been kindly provided by METEO France.

References

- Aan de Brugh, J. M. J., Henzing, J. S., Schaap, M., Morgan, W. T., van Heerwaarden, C. C., Weijers, E. P., Coe, H. and Krol, M. C.: Modelling the partitioning of ammonium nitrate in the convective boundary layer, *Atmos. Chem. Phys.*, 12(6), 3005–3023, doi:10.5194/acp-12-3005-2012, 2012.
- Airparif: Inventaire des émissions en Ile-de-France en 2005. [online] Available from: http://www.airparif.asso.fr/_pdf/publications/Rinventaire_2005_201004.pdf, 2010.
- Airparif: Origine des particules en Ile-de-France. [online] Available from: http://www.airparif.asso.fr/_pdf/publications/rapport-particules-110914.pdf, 2011.
- Airparif: Source apportionment of airborne particles in the Ile-de-France region. [online] Available from: http://www.airparif.asso.fr/_pdf/publications/rapport-particules-anglais-120829.pdf, 2012.
- Ansari, A. S. and Pandis, S. N.: Response of Inorganic PM to Precursor Concentrations, *Environ. Sci. Technol.*, 32(18), 2706–2714, doi:10.1021/es971130j, 1998.
- Asman, W. A. H., Sutton, M. A. and Schjorring, J. K.: Ammonia: emission, atmospheric transport and deposition, *New Phytol.*, 139(1), 27–48, doi:10.1046/j.1469-8137.1998.00180.x, 1998.
- Baklanov, A., Lawrence, M., Pandis, S., Mahura, A., Finardi, S., Moussiopoulos, N., Beekmann, M., Laj, P., Gomes, L., Jaffrezo, J.-L., Borbon, A., Coll, I., Gros, V., Sciare, J., Kukkonen, J., Galmarini, S., Giorgi, F., Grimmond, S., Esau, I., Stohl, A., Denby, B., Wagner, T., Butler, T., Baltensperger, U., Builtjes, P., van den Hout, D., van der Gon, H. D., Collins, B., Schlutzen, H., Kulmala, M.,

1 Zilitinkevich, S., Sokhi, R., Friedrich, R., Theloke, J., Kummer, U., Jalkinen, L., Halenka, T.,
2 Wiedensholer, A., Pyle, J. and Rossow, W. B.: MEGAPOLI: concept of multi-scale modelling of
3 megacity impact on air quality and climate, *Adv. Sci. Res.*, 4, 115–120, doi:10.5194/asr-4-115-
4 2010, 2010.

5 Bessagnet, B., Menut, L., Curci, G., Hodzic, A., Guillaume, B., Liousse, C., Moukhtar, S., Pun, B.,
6 Seigneur, C. and Schulz, M.: Regional modeling of carbonaceous aerosols over Europe - focus
7 on secondary organic aerosols, *J. Atmos. Chem.*, 61(3), 175–202, doi:10.1007/s10874-009-
8 9129-2, 2009.

9 Bishop, G. A., Peddle, A. M., Stedman, D. H. and Zhan, T.: On-road emission measurements of
10 reactive nitrogen compounds from three California cities., *Environ. Sci. Technol.*, 44(9), 3616–
11 20, doi:10.1021/es903722p, 2010.

12 Blanchard, C. L. and Hidy, G. M.: Effects of changes in sulfate, ammonia, and nitric acid on
13 particulate nitrate concentrations in the Southeastern United States, *J. Air Waste Manage.*
14 *Assoc.*, 53(3), 283–290, doi:10.1080/10473289.2003.10466152, 2003.

15 Bressi, M., Sciare, J., Gherzi, V., Bonnaire, N., Nicolas, J. B., Petit, J.-E., Moukhtar, S., Rosso, A.,
16 Mihalopoulos, N. and Féron, A.: A one-year comprehensive chemical characterisation of fine
17 aerosol (PM_{2.5}) at urban, suburban and rural background sites in the region of Paris (France),
18 *Atmos. Chem. Phys.*, 13(15), 7825–7844, doi:10.5194/acp-13-7825-2013, 2013.

19 Brook, J. R., Zhang, L., Li, Y. and Johnson, D.: Description and evaluation of a model of
20 deposition velocities for routine estimates of dry deposition over North America. Part II:
21 review of past measurements and model results, *Atmos. Environ.*, 33(30), 5053–5070,
22 doi:10.1016/S1352-2310(99)00251-4, 1999.

23 Cadle, S. ., Countess, R. . and Kelly, N. .: Nitric acid and ammonia in urban and rural locations,
24 *Atmos. Environ.*, 16(10), 2501–2506, doi:10.1016/0004-6981(82)90141-X, 1982.

25 Cadle, S. H.: Seasonal variations in nitric acid, nitrate, strong aerosol acidity, and ammonia in
26 an urban area, *Atmos. Environ.*, 19(1), 181–188, doi:10.1016/0004-6981(85)90149-0, 1985.

27 Camargo, J. A. and Alonso, A.: Ecological and toxicological effects of inorganic nitrogen
28 pollution in aquatic ecosystems: A global assessment., *Environ. Int.*, 32(6), 831–49,
29 doi:10.1016/j.envint.2006.05.002, 2006.

30 Carnevale, C., Finzi, G., Pisoni, E., Thunis, P. and Volta, M.: The impact of thermodynamic
31 module in the CTM performances, *Atmos. Environ.*, 61, 652–660,
32 doi:10.1016/j.atmosenv.2012.06.058, 2012.

33 Carslaw, D. C. and Rhys-Tyler, G.: New insights from comprehensive on-road measurements of
34 NO_x, NO₂ and NH₃ from vehicle emission remote sensing in London, UK, *Atmos. Environ.*, 81,
35 339–347, doi:10.1016/j.atmosenv.2013.09.026, 2013.

36 Chow, J. C.: Health Effects of Fine Particulate Air Pollution: Lines that Connect, *J. Air Waste*
37 *Manage. Assoc.*, 56(6), 707–708, doi:10.1080/10473289.2006.10464484, 2006.

38 CITEPA: Inventaire des émissions de polluants atmosphériques et de gaz à effet de serre en
39 France - Séries sectorielles et analyses étendues., 2013.

40 Clarisse, L., Clerbaux, C., Dentener, F., Hurtmans, D. and Coheur, P.-F.: Global ammonia
41 distribution derived from infrared satellite observations, *Nat. Geosci.*, 2(7), 479–483,
42 doi:10.1038/ngeo551, 2009.

43 Clarisse, L., Shephard, M. W., Dentener, F., Hurtmans, D., Cady-Pereira, K., Karagulian, F., Van
44 Damme, M., Clerbaux, C. and Coheur, P.-F.: Satellite monitoring of ammonia: A case study of
45 the San Joaquin Valley, *J. Geophys. Res.*, 115(D13302), doi:10.1029/2009JD013291, 2010.

46 Dall'Osto, M., Harrison, R. M., Coe, H. and Williams, P.: Real-time secondary aerosol formation
47 during a fog event in London, *Atmos. Chem. Phys.*, 9(7), 2459–2469, doi:10.5194/acp-9-2459-
48 2009, 2009.

49 Davidson, C. I. and Wu, Y. L.: Dry deposition of particle and vapors, in S. E. Lindberg, A. L. Page
50 and S. A. Norton (ads.): *Acidic precipitation (vol. 3)*. Springer Verlag, New York, pp. 103–216.,
51 1990.

52 Deguillaume, L., Beekmann, M. and Menut, L.: Bayesian Monte Carlo analysis applied to
53 regional-scale inverse emission modeling for reactive trace gases, *J. Geophys. Res.*,

1 112(D02307), doi:10.1029/2006JD007518, 2007.

2 Development, U., Kuenen, J., Gon, H. D. Van Der, Visschedijk, A. and Brugh, V. Der: MACC
3 European emission inventory for the years 2003-2007, 2011.

4 Erisman, J. W., Van Pul, A. and Wyers, P.: Parametrization of surface resistance for the
5 quantification of atmospheric deposition of acidifying pollutants and ozone, *Atmos. Environ.*,
6 28(16), 2595–2607, doi:10.1016/1352-2310(94)90433-2, 1994.

7 Erisman, J. W., Otjes, R., Hensen, A., Jongejan, P., van den Bulk, P., Khlystov, A., Möls, H. and
8 Slanina, S.: Instrument development and application in studies and monitoring of ambient
9 ammonia, *Atmos. Environ.*, 35(11), 1913–1922, doi:10.1016/S1352-2310(00)00544-6, 2001.

10 Folberth, G. A., Hauglustaine, D. A., Lathière, J. and Brocheton, F.: Interactive chemistry in the
11 Laboratoire de Météorologie Dynamique general circulation model: model description and
12 impact analysis of biogenic hydrocarbons on tropospheric chemistry, *Atmos. Chem. Phys.*,
13 6(8), 2273–2319, doi:10.5194/acp-6-2273-2006, 2006.

14 Fountoukis, C. and Nenes, A.: ISORROPIA II: a computationally efficient thermodynamic
15 equilibrium model for K^+ - Ca^{2+} - Mg^{2+} - NH_4^+ - Na^+ - SO_4^{2-} - NO_3^- - Cl^- - H_2O aerosols, *Atmos.*
16 *Chem. Phys.*, 7(17), 4639–4659, doi:10.5194/acp-7-4639-2007, 2007.

17 Freney, E. J., Sellegri, K., Canonaco, F., Colomb, A., Borbon, A., Michoud, V., Doussin, J.-F.,
18 Crumeyrolle, S., Amarouche, N., Pichon, J.-M., Bourianne, T., Gomes, L., Prevot, A. S. H.,
19 Beekmann, M. and Schwarzenböck, A.: Characterizing the impact of urban emissions on
20 regional aerosol particles: airborne measurements during the MEGAPOLI experiment, *Atmos.*
21 *Chem. Phys.*, 14(3), 1397–1412, doi:10.5194/acp-14-1397-2014, 2014.

22 Garcia, L., Bedos, C., Générumont, S., Braud, I. and Cellier, P.: Assessing the ability of mechanistic
23 volatilization models to simulate soil surface conditions: a study with the Volt'Air model, *Sci.*
24 *Total Environ.*, 409(19), 3980–92, doi:10.1016/j.scitotenv.2011.05.003, 2011.

25 Générumont, S. and Cellier, P.: A mechanistic model for estimating ammonia volatilization from
26 slurry applied to bare soil, *Agric. For. Meteorol.*, 88(1-4), 145–167, doi:10.1016/S0168-
27 1923(97)00044-0, 1997.

28 Gon, H. D. Van Der, Visschedijk, A. and Appelhans, F. J.: A high resolution European emission
29 data base for the year 2005. [online] Available from:
30 http://www.csb.gov.tr/db/necen/editordosya/file/NEC/MACC_Training/TNO_PAREST.pdf,
31 2010.

32 Gong, L., Lewicki, R., Griffin, R. J., Flynn, J. H., Lefer, B. L. and Tittel, F. K.: Atmospheric ammonia
33 measurements in Houston, TX using an external-cavity quantum cascade laser-based sensor,
34 *Atmos. Chem. Phys.*, 11(18), 9721–9733, doi:10.5194/acp-11-9721-2011, 2011.

35 Grantz, D. A., Garner, J. H. B. and Johnson, D. W.: Ecological effects of particulate matter.,
36 *Environ. Int.*, 29(2-3), 213–39, doi:10.1016/S0160-4120(02)00181-2, 2003.

37 Guenther, A., Karl, T., Harley, P., Wiedinmyer, C., Palmer, P. I. and Geron, C.: Estimates of global
38 terrestrial isoprene emissions using MEGAN (Model of Emissions of Gases and Aerosols from
39 Nature), *Atmos. Chem. Phys. Discuss.*, 6(1), 107–173, doi:10.5194/acpd-6-107-2006, 2006.

40 Haeffelin, M., Angelini, F., Morille, Y., Martucci, G., Frey, S., Gobbi, G. P., Lolli, S., O'Dowd, C. D.,
41 Sauvage, L., Xueref-Rémy, I., Wastine, B. and Feist, D. G.: Evaluation of Mixing-Height
42 Retrievals from Automatic Profiling Lidars and Ceilometers in View of Future Integrated
43 Networks in Europe, *Boundary-Layer Meteorol.*, 143(1), 49–75, doi:10.1007/s10546-011-
44 9643-z, 2012.

45 Hamaoui-Laguel, L., Meleux, F., Beekmann, M., Bessagnet, B., Générumont, S., Cellier, P. and
46 Létinois, L.: Improving ammonia emissions in air quality modelling for France, *Atmos.*
47 *Environ.*, 92, 584–595, doi:10.1016/j.atmosenv.2012.08.002, 2014.

48 Hansen, M. C., Defries, R. S., Townshend, J. R. G. and Sohlberg, R.: Global land cover
49 classification at 1 km spatial resolution using a classification tree approach, *Int. J. Remote*
50 *Sens.*, 21(6-7), 1331–1364, doi:10.1080/014311600210209, 2000.

51 Harrison, R. M. and Pio, C. A.: Size-differentiated composition of inorganic atmospheric
52 aerosols of both marine and polluted continental origin, *Atmos. Environ.*, 17(9), 1733–1738,
53 doi:10.1016/0004-6981(83)90180-4, 1983.

1 Hass, H., Van Loon, M., Kessler, C., Stern, R., Matthijsen, J., Sauter, F., Zlatev, Z., Langner, J.,
2 Foltescu, V. and Schaap, M.: Aerosol modelling: results and intercomparison from European
3 regional scale modeling systems., 2003.

4 Hauglustaine, D. a.: Interactive chemistry in the Laboratoire de Météorologie Dynamique
5 general circulation model: Description and background tropospheric chemistry evaluation, J.
6 Geophys. Res., 109(D4), D04314, doi:10.1029/2003JD003957, 2004.

7 Healy, R. M., Sciare, J., Poulain, L., Kamili, K., Merkel, M., Müller, T., Wiedensohler, A., Eckhardt,
8 S., Stohl, A., Sarda-Estève, R., McGillicuddy, E., O'Connor, I. P., Sodeau, J. R. and Wenger, J. C.:
9 Sources and mixing state of size-resolved elemental carbon particles in a European megacity:
10 Paris, Atmos. Chem. Phys., 12(4), 1681–1700, doi:10.5194/acp-12-1681-2012, 2012.

11 IPCC: Climate change 2013 : The physical science basis. [online] Available from:
12 <http://www.ipcc.ch/report/ar5/wg1/>, 2013.

13 Kanaya, Y., Cao, R., Akimoto, H., Fukuda, M., Komazaki, Y., Yokouchi, Y., Koike, M., Tanimoto, H.,
14 Takegawa, N. and Kondo, Y.: Urban photochemistry in central Tokyo: 1. Observed and
15 modeled OH and HO₂ radical concentrations during the winter and summer of 2004, J.
16 Geophys. Res., 112(D21312), doi:10.1029/2007JD008670, 2007.

17 Kean, A. J., Littlejohn, D., Ban-Weiss, G. A., Harley, R. A., Kirchstetter, T. W. and Lunden, M. M.:
18 Trends in on-road vehicle emissions of ammonia, Atmos. Environ., 43(8), 1565–1570,
19 doi:10.1016/j.atmosenv.2008.09.085, 2009.

20 Kim, Y., Couvidat, F., Sartelet, K. and Seigneur, C.: Comparison of different gas-phase
21 mechanisms and aerosol modules for simulating particulate matter formation, J. Air Waste
22 Manage. Assoc., 61, 1218–1226, 2011.

23 Konovalov, I. B., Beekmann, M., Richter, a. and Burrows, J. P.: Inverse modelling of the spatial
24 distribution of NO_x emissions on a continental scale using satellite data, Atmos. Chem. Phys.,
25 6(7), 1747–1770, doi:10.5194/acp-6-1747-2006, 2006.

26 Kuenen, J. J. P., Visschedijk, A. J. H., Jozwicka, M. and Denier van der Gon, H. A. C.: TNO-MACC_II
27 emission inventory; a multi-year (2003–2009) consistent high-resolution European emission
28 inventory for air quality modelling, Atmos. Chem. Phys., 14(20), 10963–10976,
29 doi:10.5194/acp-14-10963-2014, 2014.

30 Lombardo, T., Gentaz, L., Verney-Carron, A., Chabas, A., Loisel, C., Neff, D. and Leroy, E.:
31 Characterisation of complex alteration layers in medieval glasses, Corros. Sci., 72, 10–19,
32 doi:10.1016/j.corsci.2013.02.004, 2013.

33 Ma, B. L., Wu, T. Y., Tremblay, N., Deen, W., McLaughlin, N. B., Morrison, M. J. and Stewart, G.:
34 On-Farm Assessment of the Amount and Timing of Nitrogen Fertilizer on Ammonia
35 Volatilization, Agron. J., 102(1), 134–144, doi:10.2134/agronj2009.0021, 2010.

36 Massad, R.-S., Nemitz, E. and Sutton, M. A.: Review and parameterisation of bi-directional
37 ammonia exchange between vegetation and the atmosphere, Atmos. Chem. Phys., 10(21),
38 10359–10386, doi:10.5194/acp-10-10359-2010, 2010.

39 Mather, T. A., Allen, A. G., Davison, B. M., Pyle, D. M., Oppenheimer, C. and McGonigle, A. J. S.:
40 Nitric acid from volcanoes, Earth Planet. Sci. Lett., 218(1-2), 17–30, doi:10.1016/S0012-
41 821X(03)00640-X, 2004.

42 Matsumoto, K. and Tanaka, H.: Formation and dissociation of atmospheric particulate nitrate
43 and chloride: An approach based on phase equilibrium, Atmos. Environ., 30(4), 639–648,
44 doi:10.1016/1352-2310(95)00290-1, 1996.

45 Menut, L., Bessagnet, B., Khvorostyanov, D., Beekmann, M., Blond, N., Colette, a., Coll, I., Curci,
46 G., Foret, G., Hodzic, a., Mailler, S., Meleux, F., Monge, J.-L., Pison, I., Siour, G., Turquety, S.,
47 Valari, M., Vautard, R. and Vivanco, M. G.: CHIMERE 2013: a model for regional atmospheric
48 composition modelling, Geosci. Model Dev., 6(4), 981–1028, doi:10.5194/gmd-6-981-2013,
49 2013.

50 Michoud, V., Kukui, A., Camredon, M., Colomb, A., Borbon, A., Miet, K., Aumont, B., Beekmann,
51 M., Durand-Jolibois, R., Perrier, S., Zapf, P., Siour, G., Ait-Helal, W., Locoge, N., Sauvage, S., Afif,
52 C., Gros, V., Furger, M., Ancellet, G. and Doussin, J. F.: Radical budget analysis in a suburban
53 European site during the MEGAPOLI summer field campaign, Atmos. Chem. Phys., 12(24),

11951–11974, doi:10.5194/acp-12-11951-2012, 2012.

Moya, M., Ansari, A. S. and Pandis, S. N.: Partitioning of nitrate and ammonium between the gas and particulate phases during the 1997 IMADA-AVER study in Mexico City, *Atmos. Environ.*, 35(10), 1791–1804, doi:10.1016/S1352-2310(00)00292-2, 2001.

Mozurkewich, M.: The dissociation constant of ammonium nitrate and its dependence on temperature, relative humidity and particle size, *Atmos. Environ. Part A. Gen. Top.*, 27(2), 261–270, doi:10.1016/0960-1686(93)90356-4, 1993.

Mulawa, P. A., Cadle, S. H., Lipari, F., Ang, C. C. and Vandervennet, R.: Urban dew: Its composition and influence on dry deposition rates, *Atmos. Environ.*, 20(7), 1389–1396, doi:10.1016/0004-6981(86)90009-0, 1986.

Nenes, A., Pandis, S. and Pilinis, C.: ISORROPIA : A New Thermodynamic Equilibrium Model for Multiphase Multicomponent Inorganic Aerosols, *Aquat. geochemistry*, 4(1), 123–152 [online] Available from: <http://link.springer.com/article/10.1023/A%3A1009604003981> (Accessed 29 April 2013), 1998.

Nenes, A., Pandis, S. N. and Pilinis, C.: Continued development and testing of a new thermodynamic aerosol module for urban and regional air quality models, *Atmos. Environ.*, 33(10), 1553–1560, doi:10.1016/S1352-2310(98)00352-5, 1999.

Neuman, J. A., Huey, L. G., Ryerson, T. B. and Fahey, D. W.: Study of inlet materials for sampling atmospheric nitric acid, *Environ. Sci. Technol.*, 33(7), 1133–1136, doi:10.1021/es980767f, 1999.

Norman, M., Spirig, C., Wolff, V., Trebs, I., Flechard, C., Wisthaler, A., Schnitzhofer, R., Hansel, A. and Neftel, A.: Intercomparison of ammonia measurement techniques at an intensively managed grassland site (Oensingen, Switzerland), *Atmos. Chem. Phys.*, 9(8), 2635–2645, doi:10.5194/acp-9-2635-2009, 2009.

Ottley, C. J. and Harrison, R. M.: The spatial distribution and particle size of some inorganic nitrogen, sulphur and chlorine species over the North Sea, *Atmos. Environ. Part A. Gen. Top.*, 26(9), 1689–1699, doi:10.1016/0960-1686(92)90067-U, 1992.

Pang, Y., Eatough, N. L., Wilson, J. and Eatough, D. J.: Effect of Semivolatile Material on PM_{2.5} Measurement by the PM_{2.5} Federal Reference Method Sampler at Bakersfield, California, *Aerosol Sci. Technol.*, 36(3), 289–299, doi:10.1080/027868202753504489, 2002.

Parmar, R. ., Satsangi, G. ., Lakhani, A., Srivastava, S. . and Prakash, S.: Simultaneous measurements of ammonia and nitric acid in ambient air at Agra (27°10'N and 78°05'E) (India), *Atmos. Environ.*, 35(34), 5979–5988, doi:10.1016/S1352-2310(00)00394-0, 2001.

Pay, M. T., Jiménez-Guerrero, P. and Baldasano, J. M.: Assessing sensitivity regimes of secondary inorganic aerosol formation in Europe with the CALIOPE-EU modeling system, *Atmos. Environ.*, 51, 146–164, doi:10.1016/j.atmosenv.2012.01.027, 2012.

Perrino, C., Catrambone, M., Di Menno Di Bucchianico, A. and Allegrini, I.: Gaseous ammonia in the urban area of Rome, Italy and its relationship with traffic emissions, *Atmos. Environ.*, 36(34), 5385–5394, doi:10.1016/S1352-2310(02)00469-7, 2002.

Petetin, H., Beekmann, M., Sciare, J., Bressi, M., Rosso, A., Sanchez, O. and Gherzi, V.: A novel model evaluation approach focusing on local and advected contributions to urban PM_{2.5} levels – application to Paris, France, *Geosci. Model Dev.*, 7(4), 1483–1505, doi:10.5194/gmd-7-1483-2014, 2014.

Petit, J.-E., Favez, O., Sciare, J., Crenn, V., Sarda-Estève, R., Bonnaire, N., Močnik, G., Dupont, J.-C., Haeffelin, M. and Leoz-Garziandia, E.: Two years of near real-time chemical composition of submicron aerosols in the region of Paris using an Aerosol Chemical Speciation Monitor (ACSM) and a multi-wavelength Aethalometer, *Atmos. Chem. Phys.*, 15(6), 2985–3005, doi:10.5194/acp-15-2985-2015, 2015.

Pierson, W. R., Brachaczek, W. W., Japar, S. M., Cass, G. R. and Solomon, P. A.: Dry deposition and dew chemistry in Claremont, California, during the 1985 nitrogen species methods comparison study, *Atmos. Environ.*, 22(8), 1657–1663, doi:10.1016/0004-6981(88)90393-9, 1988.

Platt, U., Perner, D., Schröder, J., Kessler, C. and Toenissen, A.: The diurnal variation of NO₃, J.

1 Geophys. Res., 86, 11965–11970, 1981.

2 Pleim, J. E., Bash, J. O., Walker, J. T. and Cooter, E. J.: Development and evaluation of an
3 ammonia bidirectional flux parameterization for air quality models, *J. Geophys. Res. Atmos.*,
4 118(9), 3794–3806, doi:10.1002/jgrd.50262, 2013.

5 Pope, C. A., Ezzati, M. and Dockery, D. W.: Fine-particulate air pollution and life expectancy in
6 the United States., *N. Engl. J. Med.*, 360(4), 376–86, doi:10.1056/NEJMsa0805646, 2009.

7 Pouliot, G., Pierce, T., Denier van der Gon, H., Schaap, M., Moran, M. and Nopmongkol, U.:
8 Comparing emission inventories and model-ready emission datasets between Europe and
9 North America for the AQMEII project, *Atmos. Environ.*, 53, 4–14,
10 doi:10.1016/j.atmosenv.2011.12.041, 2012.

11 Putaud, J.-P., Van Dingenen, R., Alastuey, A., Bauer, H., Birmili, W., Cyrys, J., Flentje, H., Fuzzi, S.,
12 Gehrig, R., Hansson, H. C., Harrison, R. M., Herrmann, H., Hitzenberger, R., Hüglin, C., Jones, A.
13 M., Kasper-Giebl, A., Kiss, G., Kousa, A., Kuhlbusch, T. a. J., Löschau, G., Maenhaut, W., Molnar,
14 A., Moreno, T., Pekkanen, J., Perrino, C., Pitz, M., Puxbaum, H., Querol, X., Rodriguez, S., Salma, I.,
15 Schwarz, J., Smolik, J., Schneider, J., Spindler, G., ten Brink, H., Tursic, J., Viana, M.,
16 Wiedensohler, A. and Raes, F.: A European aerosol phenomenology - 3 : Physical and chemical
17 characteristics of particulate matter from 60 rural, urban, and kerbside sites across Europe,
18 *Atmos. Environ.*, 44(10), 1308–1320, doi:10.1016/j.atmosenv.2009.12.011, 2010.

19 Reche, C., Viana, M., Pandolfi, M., Alastuey, A., Moreno, T., Amato, F., Ripoll, A. and Querol, X.:
20 Urban NH₃ levels and sources in a Mediterranean environment, *Atmos. Environ.*, 57, 153–164,
21 doi:10.1016/j.atmosenv.2012.04.021, 2012.

22 Sartelet, K., Debry, E., Fahey, K., Roustan, Y., Tombette, M. and Sportisse, B.: Simulation of
23 aerosols and gas-phase species over Europe with the Polyphemus system: Part I - Model-to-
24 data comparison for 2001, *Atmos. Environ.*, 41(29), 6116–6131,
25 doi:10.1016/j.atmosenv.2007.04.024, 2007.

26 Schaap, M., Timmermans, R. M. A., Roemer, M., Boersen, G. A. C., Builtjes, P. J. H., Sauter, F. J.,
27 Velders, G. J. M. and Beck, J. P.: The LOTOS EUROS model: description, validation and latest
28 developments, *Int. J. Environ. Pollut.*, 32(2), 270, doi:10.1504/IJEP.2008.017106, 2008.

29 Schmidt, H. and Derognat, C.: A comparison of simulated and observed ozone mixing ratios for
30 the summer of 1998 in Western Europe, *Atmos. Environ.*, 35, 6277–6297 [online] Available
31 from: <http://www.sciencedirect.com/science/article/pii/S1352231001004514> (Accessed 29
32 April 2013), 2001.

33 Sciare, J., d'Argouges, O., Zhang, Q. J., Sarda-Estève, R., Gaimoz, C., Gros, V., Beekmann, M. and
34 Sanchez, O.: Comparison between simulated and observed chemical composition of fine
35 aerosols in Paris (France) during springtime: contribution of regional versus continental
36 emissions, *Atmos. Chem. Phys.*, 10(24), 11987–12004, doi:10.5194/acp-10-11987-2010,
37 2010.

38 Sciare, J., D'Argouges, O., Sarda-Estève, R., Gaimoz, C., Dolgorouky, C., Bonnaire, N., Favez, O.,
39 Bonsang, B. and Gros, V.: Large contribution of water-insoluble secondary organic aerosols in
40 the region of Paris (France) during wintertime, *J. Geophys. Res.*, 116(D22203),
41 doi:10.1029/2011JD015756, 2011.

42 Seinfeld, J. H. and Pandis, S. N.: *Atmospheric Chemistry and Physics: From Air Pollution to*
43 *Climate Change*, John Wiley, New York., 2006.

44 Skjøth, C. A., Geels, C., Berge, H., Gyldenkerne, S., Fagerli, H., Ellermann, T., Frohn, L. M.,
45 Christensen, J., Hansen, K. M., Hansen, K. and Hertel, O.: Spatial and temporal variations in
46 ammonia emissions – a freely accessible model code for Europe, *Atmos. Chem. Phys.*, 11(11),
47 5221–5236, doi:10.5194/acp-11-5221-2011, 2011.

48 Solomon, P. A., Salmon, L. G., Fall, T. and Cass, G. R.: Spatial and temporal distribution of
49 atmospheric nitric acid and particulate nitrate concentrations in the Los Angeles area,
50 *Environ. Sci. Technol.*, 26(8), 1594–1601, doi:10.1021/es00032a016, 1992.

51 Stern, R.: *Entwicklung und Anwendung des chemischen Transportmodells REM/CALGRID.*
52 *Breichte zum UBA Forschungsvorhaben 298 41 252*, Freie Universität Berlin, Institut für
53 Meteorologie., 2003.

1 Stohl, A., Haimberger, L., Scheele, M. P. and Wernli, H.: An intercomparison of results from
2 three trajectory models, *Meteorol. Appl.*, 8(2), 127–135, doi:10.1017/S1350482701002018,
3 2001.

4 Sutton, M. ., Dragosits, U., Tang, Y. . and Fowler, D.: Ammonia emissions from non-agricultural
5 sources in the UK, *Atmos. Environ.*, 34(6), 855–869, doi:10.1016/S1352-2310(99)00362-3,
6 2000.

7 Takahama, S., Wittig, A. E., Vayenas, D. V., Davidson, C. I. and Pandis, S. N.: Modeling the diurnal
8 variation of nitrate during the Pittsburgh Air Quality Study, *J. Geophys. Res.*, 109(D16),
9 D16S06, doi:10.1029/2003JD004149, 2004.

10 Trebs, I., Meixner, F. X., Slanina, J., Otjes, R., Jongejan, P. and Andreae, M. O.: Real-time
11 measurements of ammonia, acidic trace gases and water-soluble inorganic aerosol species at a
12 rural site in the Amazon Basin, *Atmos. Chem. Phys.*, 4(4), 967–987, doi:10.5194/acp-4-967-
13 2004, 2004.

14 Trebs, I., Andreae, M. O., Elbert, W., Mayol-Bracero, O. L., Soto-García, L. L., Rudich, Y.,
15 Falkovich, A. H., Maenhaut, W., Artaxo, P., Otjes, R. and Slanina, J.: Aerosol inorganic
16 composition at a tropical site: discrepancies between filter-based sampling and a semi-
17 continuous method, *Aerosol Sci. Technol.*, 42(4), 255–269,
18 doi:10.1080/02786820801992899, 2008.

19 Vayenas, D. V., Takahama, S., Davidson, C. I. and Pandis, S. N.: Simulation of the
20 thermodynamics and removal processes in the sulfate-ammonia-nitric acid system during
21 winter: Implications for PM_{2.5} control strategies, *J. Geophys. Res.*, 110(D7), D07S14,
22 doi:10.1029/2004JD005038, 2005.

23 Vrekoussis, M., Kanakidou, M., Mihalopoulos, N., Crutzen, P. J., Lelieveld, J., Perner, D.,
24 Berresheim, H. and Baboukas, E.: Role of the NO₃ radicals in oxidation processes in the
25 eastern Mediterranean troposphere during the MINOS campaign, *Atmos. Chem. Phys.*, 4(1),
26 169–182, doi:10.5194/acp-4-169-2004, 2004.

27 Wesely, M. L.: Parameterization of surface resistances to gaseous dry deposition in regional-
28 scale numerical models, *Atmos. Environ.*, 23(6), 1293–1304, doi:10.1016/0004-
29 6981(89)90153-4, 1989.

30 Wichink Kruit, R. J. (Roy), van Pul, W. A. J., Otjes, R. P., Hofschreuder, P., Jacobs, A. F. G. and
31 Holtslag, A. A. M.: Ammonia fluxes and derived canopy compensation points over non-
32 fertilized agricultural grassland in The Netherlands using the new gradient ammonia—high
33 accuracy—monitor (GRAHAM), *Atmos. Environ.*, 41(6), 1275–1287,
34 doi:10.1016/j.atmosenv.2006.09.039, 2007.

35 Yao, X., Hu, Q., Zhang, L., Evans, G. J., Godri, K. J. and Ng, A. C.: Is vehicular emission a significant
36 contributor to ammonia in the urban atmosphere?, *Atmos. Environ.*, 80, 499–506,
37 doi:10.1016/j.atmosenv.2013.08.028, 2013.

38 Yin, J. and Harrison, R. M.: Pragmatic mass closure study for PM_{1.0}, PM_{2.5} and PM₁₀ at
39 roadside, urban background and rural sites, *Atmos. Environ.*, 42(5), 980–988,
40 doi:10.1016/j.atmosenv.2007.10.005, 2008.

41 Zhang, L., Wright, L. P. and Asman, W. A. H.: Bi-directional air-surface exchange of atmospheric
42 ammonia: A review of measurements and a development of a big-leaf model for applications
43 in regional-scale air-quality models, *J. Geophys. Res.*, 115(D20310), 1–23,
44 doi:10.1029/2009JD013589, 2010.